TÜBİTAK

Turkish Journal of Earth Sciences

http://journals.tubitak.gov.tr/earth/

Research Article

Turkish J Earth Sci
(2016) 25: 491-512

doi:10.3906/yer-1603-11

Geochemistry of the metavolcanic rocks from the Çangaldağ Complex in the Central Pontides: implications for the Middle Jurassic arc-back-arc system in the Neotethyan Intra-Pontide Ocean

Okay ÇİMEN[1,2,*], M. Cemal GÖNCÜOĞLU[1], Kaan SAYIT[1]

[1]Department of Geological Engineering, Middle East Technical University, Ankara, Turkey
[2]Department of Geological Engineering, Munzur University, Tunceli, Turkey

Received: 14.03.2016 • **Accepted/Published Online:** 11.08.2016 • **Final Version:** 01.12.2016

Abstract: The Çangaldağ Complex in northern central Turkey is one of the main tectonic units of the Central Pontide Structural Complex that represents the remains of the poorly known Intra-Pontide branch of the Neotethys. It comprises low-grade metamorphic rocks of intrusive, extrusive, and volcaniclastic origin displaying a wide range of felsic to mafic compositions. Petrographically the complex consists of basalts-andesites-rhyodacites and tuffs with minor amount of gabbros and diabases. On the basis of geochemistry, the Çangaldağ samples are of subalkaline character and represented by both primitive and evolved members. All rock types are variably depleted in Nb compared to LREEs, similar to the lavas from subduction-related tectonic settings. In N-MORB normalized plots, the primitive members are separated into 3 groups on the basis of levels of enrichment. The first group is highly depleted and displays characteristics of boninitic lavas. The second group is relatively enriched compared to the first group but still more depleted than N-MORB. The third group, however, is the most enriched one among the three, whose level of enrichment is around that of N-MORB. The overall geochemical features suggest that the Çangaldağ Complex has been generated with the involvement of a subduction-modified mantle source. The chemistry of the primitive members further indicates that the melts generated for the formation of the Çangaldağ Complex probably occurred in both arc and back-arc regions above an intraoceanic subduction within the Intra-Pontide branch of the Neotethys.

Key words: Çangaldağ Complex, Central Pontides, geochemistry, arc-back-arc, Intra-Pontide Ocean

1. Introduction

Turkey is a part of the Alpine-Himalayan orogenic belt and was formed by accretion of a number of microplates (Şengör and Yılmaz, 1981) or terranes (Göncüoğlu et al., 1997, 2010; Okay and Tüysüz, 1999; Robertson et al., 2014). In NW Anatolia, the northernmost of these terranes is the İstanbul-Zonguldak Unit that is separated from the Sakarya Composite Terrane in the south by the Intra-Pontide Suture Belt (Göncüoğlu et al., 2000) in the southwest. The Kastamonu-Ilgaz Massif, a huge metamorphic body in the central part of Northern Anatolia (Figure 1), has been recognized since the 1930s as a distinct tectonic unit (e.g., von Kemnitz, 1936). In the later tectonic classifications, the unit was considered as a remnant of the Paleotethys (e.g., Şengör and Yılmaz, 1981; Okay and Tüysüz, 1999) or the Sakarya Composite Terrane (e.g., Göncüoğlu et al., 1997). Detailed field studies (e.g., Yılmaz, 1980, 1983; Tüysüz, 1985; Şengün et al., 1988; Yılmaz, 1988; Ustaömer and Robertson, 1993, 1994; Okay et al., 2006; Aygül et al., 2016), however, have shown the presence of a very complex network of different tectonic units including metamorphic and nonmetamorphic assemblages differing in age and tectonomagmatic origin (e.g., Aydın et al., 1986, 1995; Tüysüz, 1990; Ustaömer and Robertson, 1999; Göncüoğlu et al., 2012, 2014; Okay et al., 2013, 2014, 2015; Marroni et al., 2014; Okay and Nikishin, 2015; Sayit et al., 2016). In the previous studies a number of different names were used for these units, which complicates their correlation (Sayit et al., 2016).

The Çangaldağ Complex (CC; Ustaömer and Robertson, 1990) is one of these tectonic units located in the northern part of this structural complex, recently named as the Central Pontide Structural Complex (CPSC) by Tekin et al. (2012) or the Central Pontide Supercomplex by Okay et al. (2013). The CC is an arc-shaped body of approximately 50 km long and 40 km wide. It is geographically located between the subunits of the Sakarya Composite Terrane and the CPSC belonging to the Intra-Pontide Suture Belt. In addition, the absence of reliable ages and consistent petrological data for tectonomagmatic

* Correspondence: cokay@metu.edu.tr

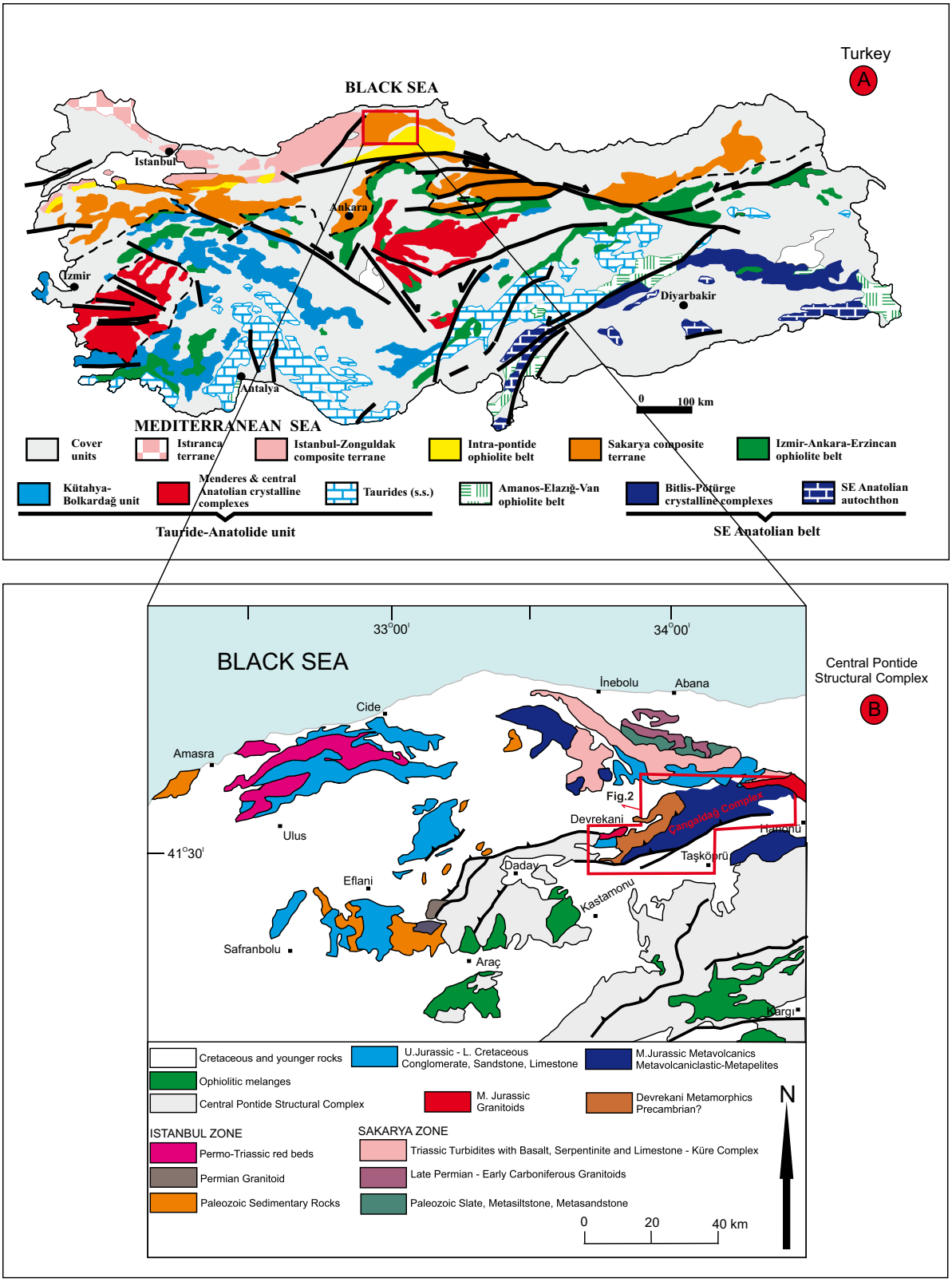

Figure 1. a) Distribution of the main alpine terranes in central North Anatolia (modified from Göncüoğlu, 2010). b) The main structural units of the Central Pontides (modified after Ustaömer and Robertson, 1999; Göncüoğlu et al., 2012, 2014; Okay et al., 2015).

classification led to conflicting proposals for the CC's organization. To mention some, a group of authors (e.g., Yılmaz, 1980, 1983; Yılmaz and Tüysüz; 1984; Şengün et al., 1988; Tüysüz, 1985, 1990; Boztuğ and Yılmaz, 1995) considered the CC as a metaophiolitic body related to the "Cimmerian" Elekdağ metaophiolite. Others (e.g., Ustaömer and Robertson, 1993, 1994, 1999) suggested that the CC was formed as a result of arc volcanism developed in the pre-Late Jurassic ocean (Paleotethys). The third view differs from the others in that the CC is the conjugate of the Nilüfer Unit of the Karakaya Complex (Okay et al., 2006). Later, this suggestion was revised by new age findings (Okay et al., 2013, 2014) as "arc-related magmatism" considering the geochemical data from Ustaömer and Robertson (1999). This brief introduction shows that the petrogenesis of the CC's metaigneous rocks and their ages are crucial for a better understanding of the interpretation of the paleotectonic setting and geological evolution of the Central Pontides.

In this paper we will describe the relations of the different metaigneous rock units, briefly report their ages, and critically evaluate the tectonomagmatic evolution of the CC by new geochemical data. The geochemical evaluation of the sources and possible igneous processes that may have generated the igneous complex together with the correlation of the surrounding metaigneous complexes in the Central Pontides will certainly provide insights to the geological evolution of this less-known area within the Northern Tethyan realm.

2. Geological framework

2.1. Regional geology

The Central Pontides consists of several tectonic units (Figure 1), such as the Küre Complex of the Sakarya Composite Terrane, Devrekani Metamorphics, Çangaldağ Pluton, CC, and Domuzdağ-Saraycık Complex (Yılmaz and Tüysüz, 1984; Ustaömer and Robertson, 1999; Kozur et al., 2000; Okay et al., 2006, 2013; Göncüoğlu et al., 2012, 2014, Aygül et al., 2016).

2.1.1. The Devrekani Metamorphics

In the modified tectonic map of the Central Pontides (Figures 2a and 2b) the Devrekani Metamorphics (DM) is located to the NW of the CC and forms the structural cover of the CC. It comprises mostly gneiss, amphibolite, and metacarbonate, which were metamorphosed under amphibolite and granulite facies conditions (Boztuğ et al., 1995; Yılmaz and Boztuğ, 1995; Ustaömer and Robertson, 1999). Two mappable units were differentiated in this metamorphic body, such as the Gürleyik Gneiss and Başakpınar Metacarbonates (Yılmaz, 1980). Yılmaz and Bonhomme (1991) suggested that the age of the Gürleyik Gneiss is approximately between Early and Middle Jurassic based upon the K-Ar mica and amphibole ages (149 Ma to 170 Ma). Later, similar Jurassic metamorphism ages, 150 Ma and 156 Ma by using the Ar-Ar method, were confirmed by Okay et al. (2014) and Gücer et al. (2016), respectively. Moreover, Gücer and Arslan (2015) suggested that the protoliths of the amphibolites, orthogneisses (Permo-Carboniferous), and paragneisses are island-arc tholeiitic basalts, I-type calc-alkaline volcanic arc granitoids, and clastic sediments (shale-wackestone), respectively. Recently, the Devrekani metamorphic rocks have been interpreted as the products of Permo-Carboniferous continental arc magmatism overprinted by the Jurassic metamorphism in the northern Central Pontides (Gücer et al., 2016).

2.1.2. The Çangaldağ Pluton

The Çangaldağ Pluton (CP) is located in the north of the CC. It covers an area of about 150 km^2. According to previous studies (Yılmaz and Boztuğ, 1986; Aydın et al., 1995), this huge body intrudes into the CC in the south and the Triassic Küre Complex in the east. It is disconformably overlain by the Upper Jurassic İnaltı Formation in several locations. The field relations suggest that the formation age of the pluton must be between Triassic and Upper Jurassic.

Particularly, the primary contact relation between the CP and CC is a matter of debate as it is covered by intense vegetation in the north of the CC. At the local scale, sharp contacts with a wide zone of mylonitic rocks between the pluton and the volcanic rocks (Figure 2b) are observed in the field. By this, the primary relation between the CP and the CC is very probably a high-angle thrust or later stage strike-slip fault of regional scale along which the plutonic rocks have been deformed and dynamo-metamorphosed. The primary contact between the CP and Küre Complex is intrusive. We confirm that the Late Jurassic İnaltı Formation disconformably overlies the CP (Figures 3a and 3b).

Three different groups of rocks were determined within the CP. These are characterized by diorites, dacite porphyries, and, to a lesser extent, granites. The dioritic rocks are surrounded by the dacite porphyries, indicating the zonal character of the intrusive suite with a more mafic core. The primary igneous mineral paragenesis of the dioritic rocks is plagioclase, biotite, amphibole, and quartz. On the other hand, the dacite porphyries are characterized by abundant phenocrystic feldspars visible to the naked eye. The pluton is intruded by a number of granitic veins (Figure 3c) that are observed in the west of the CP to the north of Süle village. This observation reveals that the granitic phases formed after the diorite emplacement. The granites include K-feldspar, quartz, and biotite. Except for mylonitic deformation zones, there is no indication for the metamorphism on the CP. The mylonitic zones are also characterized by intensive alteration and mineralization.

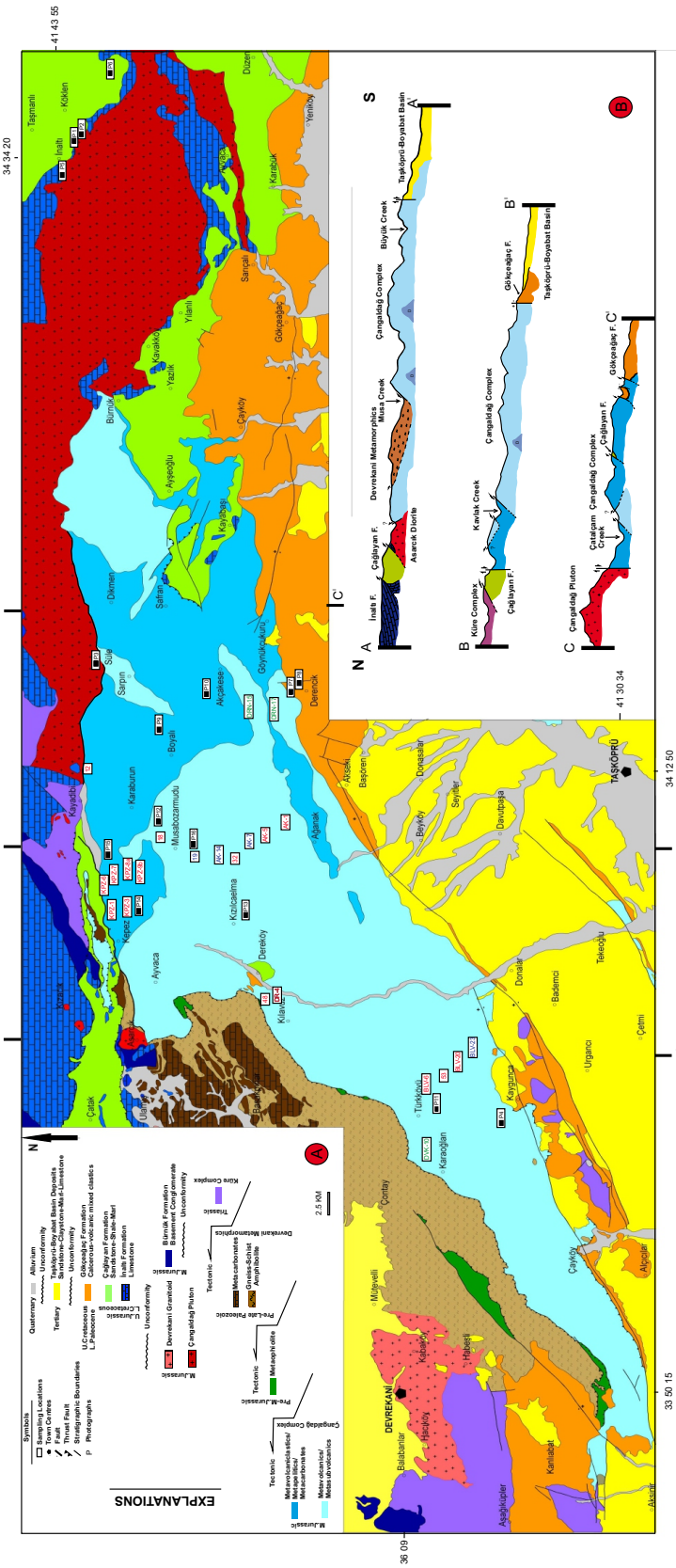

Figure 2. a) Geological map of the study area and b) cross-sections from the north to south (modified from Konya et al., 1988; blue samples: metarhyodacites, green samples: metaandesites; red samples: metabasalts/diabases).

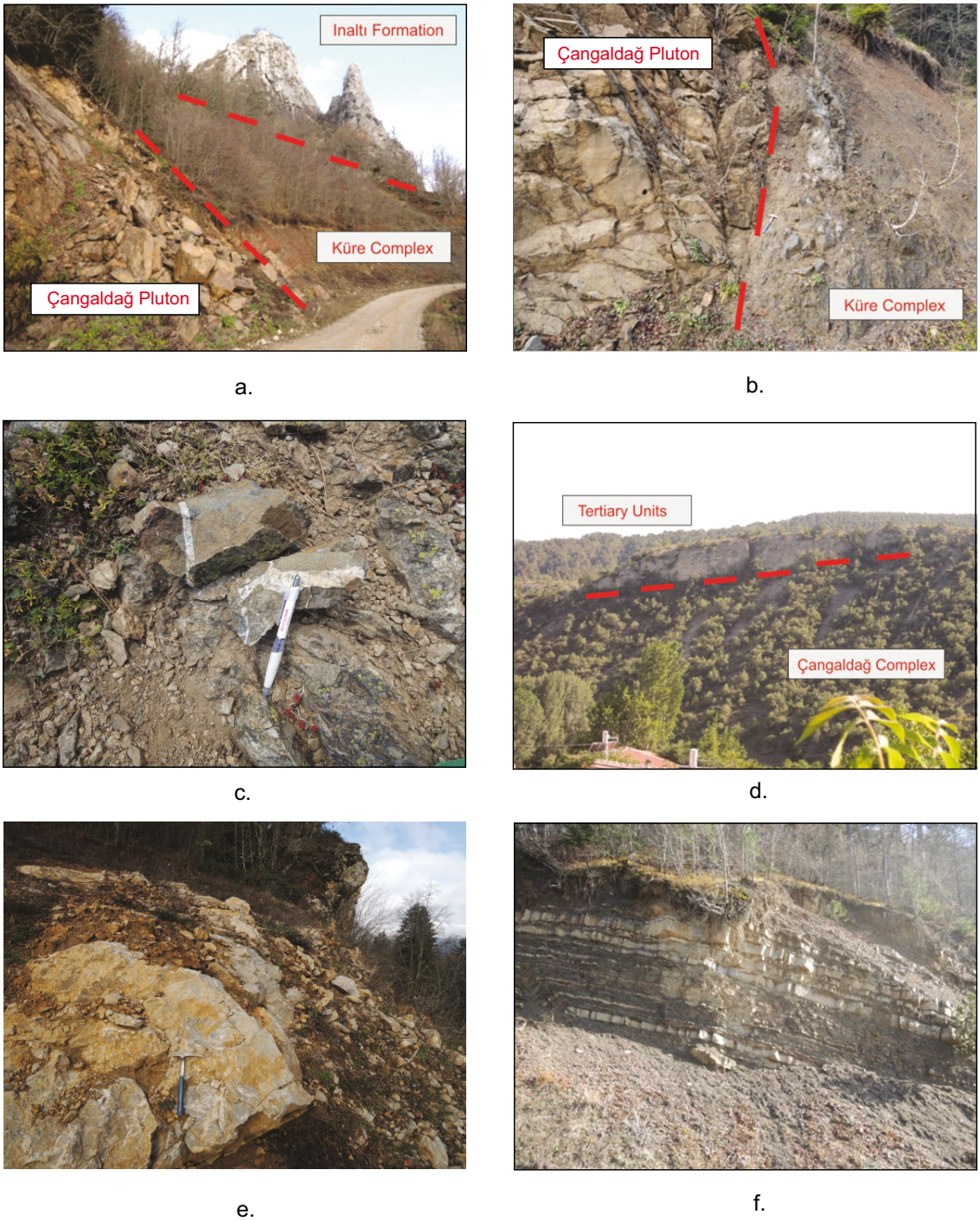

Figure 3. a) Field relations between the Çangaldağ Pluton, Küre Complex, and İnaltı formation (Locality: P1). b) Close-up image of cutting relation between Çangaldağ Pluton and Küre Complex (Locality: P2). c) The cross-cutting relation between granite veins and dioritic rock within the Çangaldağ Pluton (Locality: P3). d) Tertiary units unconformably overlay the Çangaldağ Complex (Locality: P4). e) Close-up image of the İnaltı formation (Locality: P5). f) Field image of the Çağlayan Formation (alternation of sandstone and shale; Locality: P6).

The dioritic rocks have holocrystalline/porphyritic texture, including mostly plagioclase, amphibole, and quartz phenocrysts. In relation to the dacite porphyries, they exhibit porphyritic texture as well. The phenocryst phases are embedded in a fine-grained groundmass. Plagioclase is mostly altered to sericite. The granite veins are mainly

composed of K-feldspar, plagioclase, quartz, and biotite. They display holocrystalline and porphyritic texture.

As of yet there are no published geochemical and radiometric data for this pluton in the literature. Our preliminary data (Çimen et al., 2016a) show that this intrusive body geochemically has overall subalkaline, calc-alkaline, magnesian, and I-type characteristics. It displays similar geochemical features to volcanic arc granites including LILE enrichment over HFSE coupled with negative Nb anomaly. Moreover, the pluton may have been mostly derived by partial melting of an amphibolitic (lower crustal) source.

2.1.3. The cover units

The earliest sedimentary cover of the pre-Upper Jurassic units (e.g., the CC, CP, and Küre Complex) in the region is the Late Jurassic İnaltı Formation. The İnalti Formation outcrops mainly in the north of the study area. The type locality of the formation is around İnaltı village. The thickness of this unit was measured approximately as 395 m and a shallow marine and reefal/fore-reefal character was suggested for the carbonates (Kaya and Altıner, 2014). The main lithology of the formation is the white and light gray recrystallized limestones (Figure 3e). The overlying Çağlayan formation comprises an alternation of sandstone and shale beds (Figure 3f). The sandstones are gray to yellowish in color and their thicknesses change from thin to thick, based upon the depositional environment. The shale beds are mostly thinner and of gray color. This formation unconformably overlies the CC, mostly, in the south. Şen (2013) proposed that the maximum thickness of this unit is approximately 3000 m. The Çağlayan Formation shows typical turbiditic characteristics, including graded bedding, flute casts, grooves, slump structures, etc. (Okay et al., 2013). It is unconformably overlain by the Upper Cretaceous pelagic limestones (Okay et al., 2006, 2013). In the south of the study area the Gökçeağaç Formation unconformably overlies the CC. It mainly comprises volcanoclastic rocks and calciturbidites. The volcanic clasts are generally andesitic and basaltic lavas. It also includes lithic tuff together with bands and lenses of volcaniclastic breccia. The unit mostly displays green and greenish tones. In some recent studies, this formation is assumed as a volcanic-volcanoclastic member of the Cankurtaran Formation that comprises sandstone, siltstone, claystone, and sandy limestone alternations (Uğuz and Sevin, 2007).

The Kastamonu-Boyabat Basin is bounded by the Ekinveren fault in the north (Uğuz and Sevin, 2007). Some parts of the northern margin of this basin are a reverse fault with strike-slip component, along which the CC is thrust onto the Tertiary units. The southward thrusting is also observed within the CC, which obscured the primary relations of the main rock units (Figure 2).

2.2. Çangaldağ Complex

The CC is located between the towns of Devrekani and Taşköprü (northeast of Kastamonu, Central Pontides). Okay et al. (2006) regarded this complex previously as a pre-Jurassic metabasite-phyllite-marble unit that forms several crustal-scale tectonic slices in the north and south. Ustaömer and Robertson (1999) described the complex as a structurally thickened pile of mainly volcanic rocks and subordinate volcaniclastic sedimentary rocks that overlie a basement of sheeted dykes in the north and basic extrusives in the south. The complex was also considered as a metaophiolitic body by several authors (Yılmaz, 1980, 1983; Yılmaz and Tüysüz; 1984; Tüysüz, 1985, 1990; Şengün et al., 1988; Boztuğ and Yılmaz, 1995).

The CC is mainly composed of metavolcanics, metavolcaniclastics, and metaclastic rocks. The metavolcanic rocks comprise mafic, intermediate, and felsic lavas. Additionally, some diabase dykes and pillow lavas were determined in the NE of the CC (around Karaoğlan village). Most of these magmatic rocks reflect the characteristics of the greenschist facies including epidote, actinolite, and chlorite minerals.

The primary relations between the main rock types are obscured by intense shearing and by the presence of a number of tectonic slices. Particularly, there are several thrust and strike-slip faults within the CC. They strike generally in NE-SE directions.

In previous studies, Middle Jurassic (153 Ma) and Early Cretaceous metamorphic (126–110 Ma) ages were assigned for the metabasic rocks and phyllites, respectively (Yılmaz and Bonhomme, 1991) by using mineral K-Ar methods. These Early Cretaceous metamorphic ages were confirmed by Okay et al. (2013) for the complex based upon Ar-Ar mica dating of phyllite samples (136 and 125 Ma). Recently, a single radiometric age finding for the protolith of the CC (U-Pb zircon dating from a metadacite sample) indicating a Middle Jurassic age was reported (Okay et al., 2014). Our preliminary radiometric data (in situ U-Pb dating of many zircon grains from several metadacites) confirm the Middle Jurassic magmatic ages (Çimen et al., 2016b).

2.2.1. Metaclastics and metavolcaniclastics

The metaclastic rocks within the CC consist of the pelitic and psammo-pelitic schists that occur as thick packages in the northeastern part of the study area around Karaburun and Boyalı villages. They can be easily identified by their lighter colors (white and gray, dark shades) and shiny surfaces in the field. They are highly deformed and have well-developed schistosity planes (Figure 4a). Some of them display crenulation cleavages and microfolds, which indicate the presence of multiple deformation phases (Figure 4b). Mineralogically, they are mainly made up of quartz and mica.

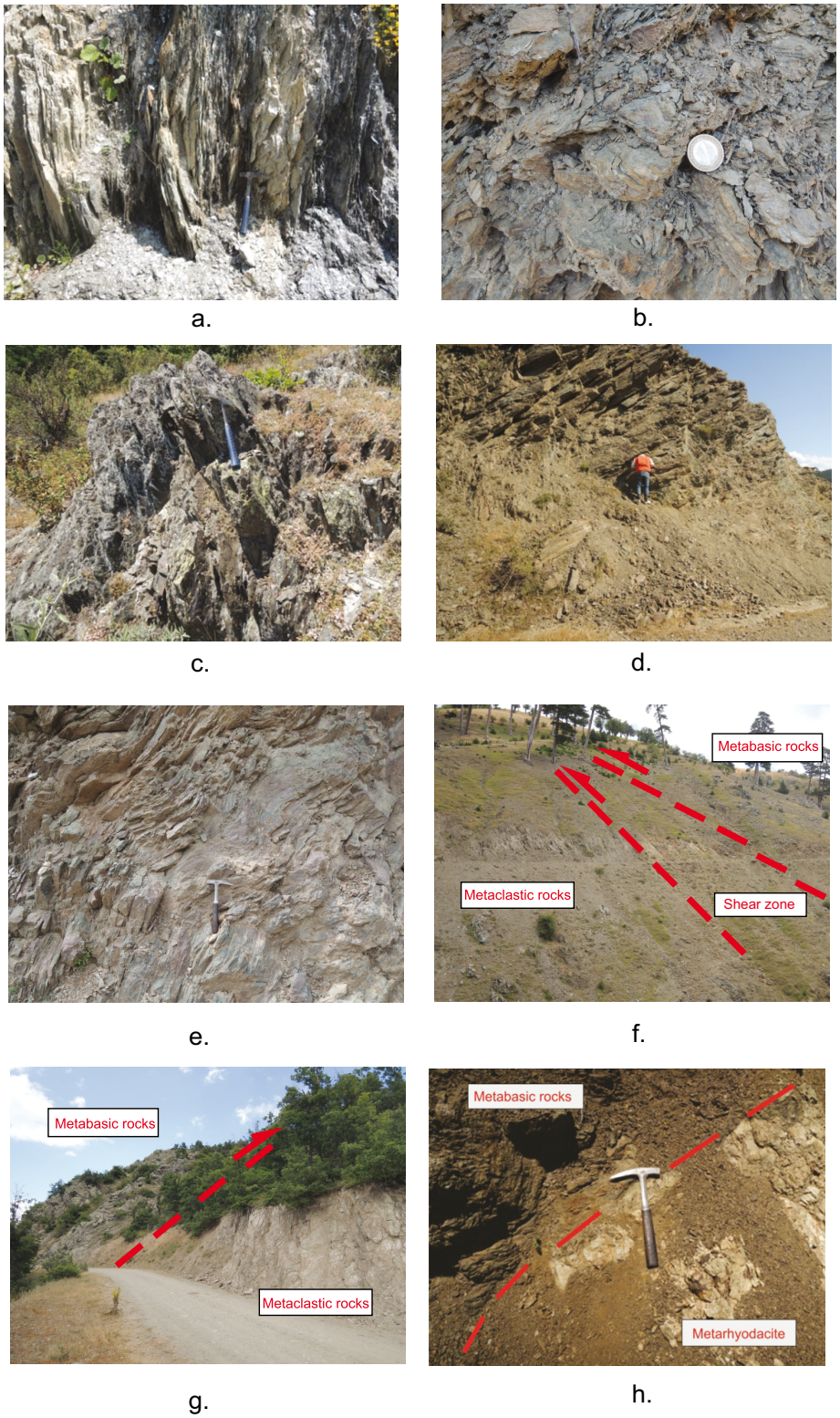

Figure 4. a) Metapelitic rocks and well-developed schistosity planes (Locality: P7). b) Microfolds of the metapelitic rocks (Locality: P8). c) Well-foliated metavolcaniclastic rocks (Locality: P9). d) Foliated metabasalts and fresh outcrops (Locality: P10). e) Field image of the folds in the metabasic rocks (Locality: P11). f) Field relation between the metavolcanic rocks and metaclastic rocks (Locality: P12). g) Field image of the relation between the metavolcanic rocks and metaclastic rocks (Locality: P13). h) The cutting relation between metarhyodacite and metabasic rocks (Locality: P14).

The metavolcaniclastic rocks are recognized by their compositional layering and alternation with the lighter colored metapelites. They form discontinuous bands and lenses within the metavolcanic lithologies. Elongated metabasic pebbles with relict volcanic texture are indicative of their volcanoclastic origin. They are dominated by epidote, actinolite, and chlorite.

2.2.2. Metavolcanics

Three different magmatic phases were determined, where the metabasalts and metaandesites/metabasaltic andesites dominate over the metarhyodacites. The metafelsic rocks are mostly observed around Musabozarmudu village in the central part of the CC. In addition to these rock types, diabase dykes and pillow lavas were locally found in the northwest of the CC around Karaoğlan village. In the field, these magmatic rocks display sharp contacts against each other (Figure 4d) and are characterized by variably intense deformation. Some of them display well-developed folding structures (Figure 4e).

The primary relationship between the basic metavolcanic and metaclastic rocks is generally obscured by intensive shearing in most outcrops (Figures 4f and 4g). However, these units are frequently cut by the felsic volcanic rocks (metarhyodacites) in different localities (for instance, south of Musabozarmudu village; Figure 4h). This significant observation reveals that the metarhyodacite rocks are relatively younger than the basic and intermediate ones within the CC.

The well-developed greenschist metamorphic paragenesis in all different metavolcanic rocks indicates that the members of this complex have undergone the same metamorphic event following their igneous formation. Most of the basic and intermediate magmatic rocks are fine-grained and include albite, epidote, actinolite and chlorite, and white mica as metamorphic minerals. The color of mafic/intermediate magmatic rocks is greenish due to the development of the secondary mineral phases. The primary mineral assemblages cannot be observed in hand-specimen size because of this metamorphic overprint. On the other hand, the felsic rocks (metarhyodacite) exhibit white and slightly brownish colors. They are highly altered. Macroscopically, the presence of resistant quartz grains helps to identify these rocks in the field.

While the well-foliated rocks display the effects of ductile deformation, the less-foliated magmatic rocks show massive original structures. Whatever the state of foliation, the metamorphic mineral paragenesis does not change dramatically.

3. Petrography

The metaigneous rocks of the CC were determined as variably deformed and metamorphosed basalts, andesites and rhyodacites, diabases, and gabbros by petrographic examination. Metabasalts have generally aphanitic/microphaneritic and porphyritic texture (Figure 5a). Rarely preserved phenocrysts are clinopyroxene, plagioclase, and few serpentinized olivines.

Clinopyroxene phenocrysts are gathered to display a glomeroporphyritic texture. They are subhedral to euhedral and marginally replaced by actinolite and chlorite. In some samples, plagioclase phenocrysts exhibit a seriate texture by the presence of randomly oriented interlocking laths. Olivine has been completely replaced by serpentine and chlorite. The metadiabases essentially comprise clinopyroxene and plagioclase. However, most of the mafic minerals have been altered to chlorite and epidote.

The primary mineral paragenesis of the metaandesites is represented mostly by plagioclase and clinopyroxene. Most of the mafic minerals have been altered to secondary metamorphic minerals such as epidote, chlorite, and actinolite, which may indicate the presence of greenschist metamorphism conditions (Figure 5b). Minerals indicating HP/LT conditions (e.g., Na-amphibole) have not been found within these metamorphic rocks.

The more felsic magmatic rocks, such as the metarhyodacites, exhibit mostly porphyritic and microcrystalline textures. The phenocryst phases are characterized by quartz and plagioclase embedded in a fine grained groundmass. They are mostly anhedral to subhedral (Figure 5c). Quartz phenocrysts display undulatory extinction and the feldspar minerals mostly have been altered to sericite. The metatuffs also display signatures of greenschist metamorphism and include chlorite, epidote, and actinolite.

The pelitic schists have very distinctive mineral paragenesis of low-grade metamorphism. They consist mostly of muscovite, biotite, feldspar, and quartz. These assemblages represent relatively aluminous compositions and the absence of garnet indicates that the metamorphism has not proceeded to medium-grade conditions. They typically have gray and black colors.

4. Geochemistry

4.1. Analytical methods

Basalt, andesite, rhyodacite, and diabase samples, collected along three traverses in the study area, were selected for geochemical analyses after petrographic observations. A total of 24 metamagmatic rock samples were geochemically analyzed at Acme Laboratories (Vancouver, Canada). Major oxides and trace-rare earth elements were analyzed using inductively coupled plasma-emission spectrometry (ICP-ES) and inductively coupled plasma-mass spectrometry (ICP-MS), respectively.

Total abundances of the major oxides and several minor elements were analyzed by lithium metaborate/tetraborate

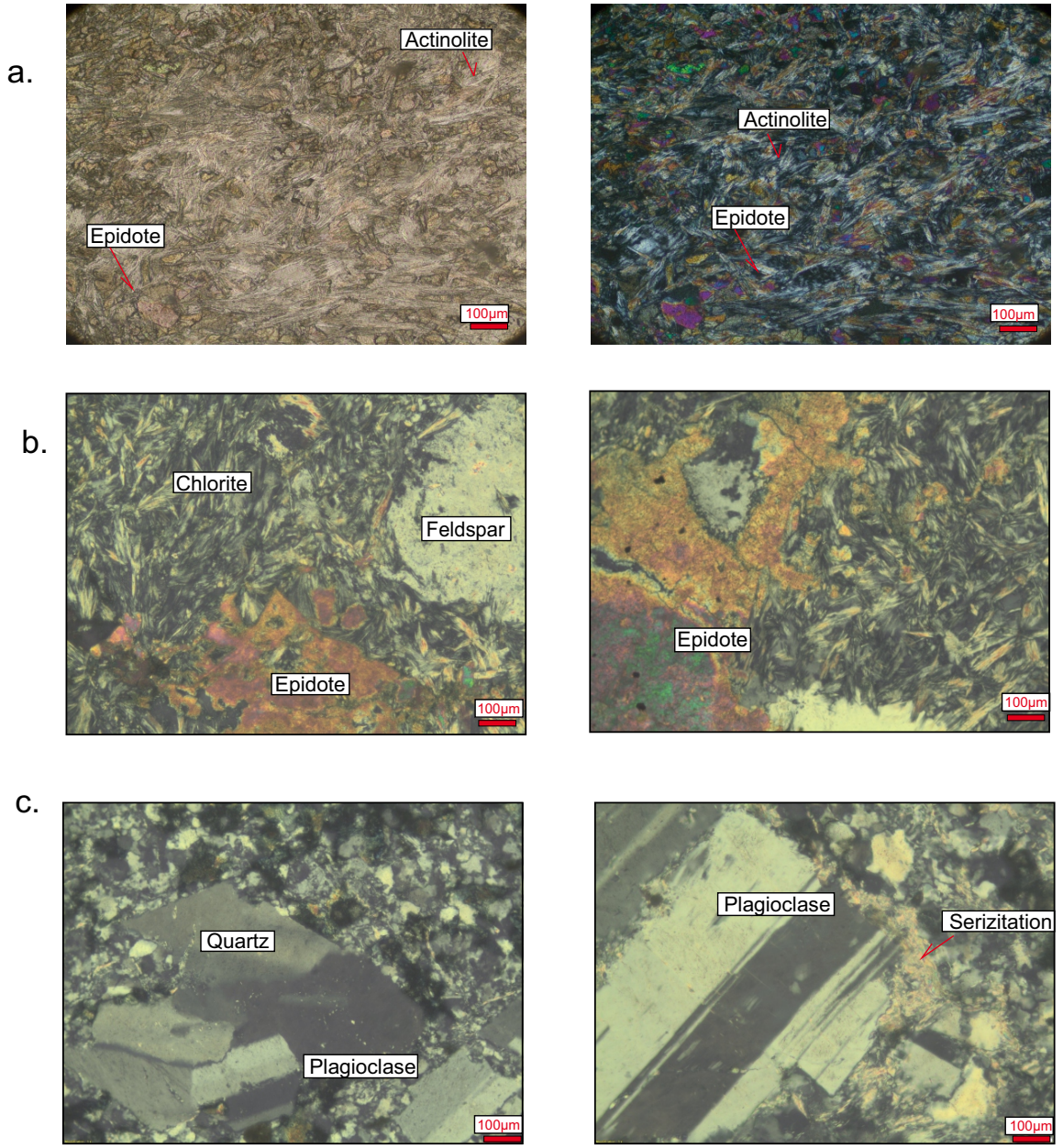

Figure 5. a) Thin-section images of metabasalt and secondary mineral assemblages. b) Thin-section images of metaandesite and mineral paragenesis. c) Thin-section images of metarhyodacite and quartz/plagioclase phenocrysts.

fusion and dilute nitric digestion. Loss on ignition (LOI) is determined by weight difference after ignition at 1000 °C. Additionally, some duplicated samples were analyzed in order to confirm the accuracy of the analyses.

4.2. Effects of the postmagmatic processes

Highly variable LOI values were observed in the metamagmatic rocks (1.4–6.0 wt. %; Table). These values may indicate the effects of both low-grade metamorphism and hydrothermal alteration as also recognized by the petrographic observations. The mobility of large ion lithophile elements (LILEs) due to postmagmatic processes is evidenced when they are plotted against Zr as displayed by the scattering of data points (Figure 6a). HFSEs and REEs, however, exhibit good correlations, indicating their immobile behavior under the secondary processes (Figure 6b). Therefore, LILEs will not be considered hereafter due to their mobile nature (Pearce, 1975; Wood et al., 1976; Floyd et al., 2000). Instead, the trace elements (Ti, Zr, rare earth elements, etc.) that are immobile under low-grade alteration/metamorphism conditions (e.g., Pearce and

Table. Major and trace element concentrations of the Çangaldağ metamagmatic rocks.

	Group 1				Group 2									Group 3				Group 4			Group 5			
Sample	DR-11	BLV-6	53	AK-5	48	KPZ-9b	12	AK-1	KPZ-3	32	BLV-20	18	DR-4	KPZ-7	KPZ-8a	KPZ-1	KPZ-6	DRN-15	DRN-17	DVK-10	BLV-23	AK-7	AK-14	19
SiO_2 (%)	46.38	54.33	56.55	48.50	51.58	46.64	45.28	48.44	50.01	44.15	48.74	46.93	57.90	47.96	47.56	47.51	48.91	59.48	63.27	51.03	76.94	77.13	78.03	75.82
Al_2O_3	15.99	13.29	12.54	15.55	17.08	18.23	13.24	17.87	15.11	18.26	16.46	16.88	14.87	15.24	16.13	15.51	15.52	14.22	14.20	15.18	12.09	11.69	11.88	12.40
Fe_2O_3	5.54	6.51	6.87	9.27	8.86	8.80	9.43	9.46	9.63	13.68	6.14	9.04	11.80	11.05	10.46	9.94	9.51	10.44	7.90	13.16	2.05	2.65	1.85	2.70
MgO	11.25	10.68	10.35	10.56	6.81	7.94	14.94	8.98	8.13	7.86	8.56	8.60	4.22	6.56	8.48	8.86	8.58	4.43	2.96	4.61	1.16	0.52	0.42	0.83
CaO	16.00	7.08	6.20	6.84	4.51	10.23	8.72	3.57	8.70	6.54	12.01	10.37	2.15	11.72	4.92	11.04	9.51	1.26	1.46	6.00	0.10	3.15	0.13	0.38
Na_2O	0.79	3.56	2.39	2.45	5.67	2.57	1.46	4.04	3.57	2.35	2.28	2.16	5.40	3.00	4.54	1.87	3.16	5.06	6.18	5.37	5.91	1.84	4.23	5.83
K_2O	0.18	0.14	0.96	2.11	0.55	0.84	0.02	1.72	0.01	1.05	1.32	0.66	0.14	0.09	0.01	0.55	0.12	0.05	0.31	0.10	0.03	1.16	0.31	0.06
TiO_2	0.17	0.26	0.18	0.36	0.60	0.77	0.67	0.72	0.71	0.68	0.65	0.95	0.82	1.38	1.24	1.04	0.91	1.28	1.11	2.07	0.15	0.16	0.22	0.25
P_2O_5	0.02	0.03	0.03	0.06	0.06	0.05	0.07	0.08	0.06	0.08	0.05	0.08	0.07	0.14	0.11	0.09	0.08	0.16	0.33	0.27	0.03	0.02	0.02	0.06
MnO	0.11	0.12	0.09	0.18	0.15	0.18	0.16	0.24	0.19	0.28	0.12	0.14	0.13	0.17	0.20	0.15	0.15	0.18	0.14	0.18	0.06	0.06	<0.01	0.05
Cr_2O_3	0.151	0.087	0.091	0.067	<0.002	0.061	0.160	0.052	0.024	0.003	0.066	0.016	<0.002	0.045	0.054	0.019	0.027	<0.002	<0.002	<0.002	<0.002	<0.002	<0.002	<0.002
LOI	3.3	3.8	3.6	3.9	4.0	3.5	5.7	4.7	3.7	4.9	3.5	4.0	2.3	2.5	6.1	3.3	3.4	3.3	2.0	1.9	1.4	1.5	2.8	1.5
Sc (ppm)	50	37	29	42	37	31	37	37	41	47	44	42	40	40	41	46	47	26	22	33	11	11	10	12
Ba	4	12	109	47	142	93	6	110	6	27	67	15	33	8	6	19	15	9	20	18	10	149	14	6
Cs	0.3	<0.1	0.6	0.5	0.1	1.6	0.2	0.5	<0.1	0.3	0.6	0.4	<0.1	0.1	<0.1	1.3	0.3	<0.1	<0.1	<0.1	<0.1	0.2	<0.1	<0.1
Hf	0.1	0.8	0.9	0.7	1.3	1.1	1.0	1.4	1.2	0.9	1.2	1.5	1.3	2.5	1.9	1.4	1.7	2.9	5.2	3.7	3.7	3.1	2.6	3.2
Nb	<0.1	0.7	0.5	0.2	0.6	0.4	0.4	0.2	0.3	0.3	0.6	0.7	0.6	1.3	1.2	0.9	0.6	2.0	4.0	3.5	1.5	1.4	1.2	1.2
Rb	4.0	1.8	22.7	29.6	3.8	21.1	<0.1	22.9	<0.1	16.3	24.1	4.0	1.1	1.3	<0.1	11.1	2.1	<0.1	3.7	<0.1	<0.1	12.8	2.6	0.1
Sr	170.1	36.4	125.9	110.7	111.1	335.7	23.4	132.6	235.6	114.3	174.4	138.2	135.8	132.3	210.3	168.4	202.1	33.5	35.5	67.9	20.0	108.1	27.1	53.8
Ta	<0.1	<0.1	<0.1	<0.1	<0.1	<0.1	<0.1	<0.1	<0.1	<0.1	<0.1	<0.1	<0.1	<0.1	<0.1	<0.1	<0.1	0.2	0.3	0.2	0.1	0.1	<0.1	<0.1
Th	<0.2	<0.2	0.4	<0.2	<0.2	<0.2	<0.2	<0.2	<0.2	<0.2	<0.2	<0.2	<0.2	<0.2	<0.2	<0.2	<0.2	0.4	<0.2	0.4	1.3	0.5	0.3	0.4
U	<0.1	<0.1	0.2	<0.1	<0.1	<0.1	<0.1	<0.1	<0.1	<0.1	<0.1	<0.1	<0.1	<0.1	<0.1	<0.1	<0.1	0.2	0.3	<0.1	0.8	<0.1	0.4	0.2
V	156	144	160	238	245	186	198	272	250	369	201	245	360	311	272	254	254	132	52	333	12	<8	13	<8
Zr	2.4	26.0	32.0	21.7	45.6	32.9	31.5	45.6	36.5	27.1	36.2	47.7	43.9	82.0	67.1	62.7	56.6	100.9	176.2	138.4	135.0	125.3	98.3	111.0
Y	4.6	4.3	5.3	8.3	15.0	16.9	14.7	16.4	17.9	12.3	13.9	18.9	18.3	29.8	23.5	20.7	21.3	36.3	52.2	36.8	31.8	29.2	16.2	26.1
Pb	0.4	0.4	0.7	0.5	0.7	0.7	0.2	0.6	0.4	0.5	0.3	0.1	0.2	0.2	0.5	0.2	0.1	1.3	0.6	0.3	0.3	0.7	0.6	0.2
Zn	9	35	31	48	59	43	42	62	41	103	33	16	78	56	75	35	38	136	100	56	50	55	17	75
Ni	48.5	119.2	163.4	73.2	19.0	163.6	224.2	98.2	36.9	23.1	62.8	32.7	4.6	68.0	148.1	35.1	37.6	1.4	3.8	7.6	0.6	3.4	0.5	1.1
La	0.1	1.7	2.4	1.8	2.6	1.1	1.7	2.6	1.8	2.2	2.1	1.8	3.0	3.1	2.8	2.2	2.3	4.8	7.3	7.7	6.1	5.3	3.3	4.7
Ce	0.4	3.8	4.8	4.0	6.2	3.4	4.3	6.2	4.5	4.3	4.9	5.9	6.3	8.8	7.4	7.0	6.3	12.6	22.8	20.7	15.4	14.0	4.9	11.8
Pr	0.09	0.47	0.54	0.49	0.90	0.65	0.71	1.03	0.73	0.67	0.71	0.95	0.93	1.58	1.27	1.18	1.13	2.05	3.55	2.96	2.06	1.96	0.74	1.71
Nd	0.8	2.3	2.6	2.3	4.4	4.0	4.1	4.8	4.4	4.0	4.1	5.8	5.3	9.8	7.0	6.9	6.4	10.5	18.3	14.3	9.7	9.4	3.5	8.3
Sm	0.30	0.33	0.53	0.78	1.62	1.71	1.44	1.73	1.50	1.27	1.45	1.84	1.53	2.98	2.25	2.21	2.32	3.74	5.89	4.29	2.80	3.07	0.79	2.36
Eu	0.23	0.12	0.23	0.29	0.53	0.68	0.64	0.66	0.54	0.54	0.55	0.74	0.55	1.13	1.04	0.88	0.92	1.30	1.76	1.76	0.61	0.70	0.28	0.54
Gd	0.64	0.62	0.74	1.16	2.27	2.39	2.05	2.28	2.18	1.71	2.20	2.76	2.51	4.34	3.50	3.25	3.21	5.42	7.80	6.05	3.49	4.14	1.44	3.26
Tb	0.13	0.13	0.14	0.21	0.43	0.44	0.37	0.41	0.43	0.33	0.38	0.53	0.48	0.79	0.66	0.57	0.61	1.01	1.45	1.11	0.69	0.77	0.33	0.61
Dy	0.85	0.76	0.91	1.31	2.73	3.03	2.64	2.68	2.97	2.18	2.31	3.25	3.21	5.11	4.55	3.72	3.84	6.90	9.32	6.31	4.55	4.68	2.55	4.04
Ho	0.18	0.16	0.20	0.33	0.54	0.64	0.53	0.51	0.56	0.44	0.51	0.73	0.67	1.05	0.91	0.76	0.77	1.47	1.88	1.40	1.10	1.06	0.64	0.96
Er	0.56	0.56	0.62	0.90	1.75	1.87	1.79	1.72	2.12	1.32	1.49	1.88	2.16	3.43	2.80	2.15	2.48	4.37	5.77	4.27	3.51	3.42	2.45	3.27
Tm	0.08	0.11	0.10	0.14	0.26	0.30	0.24	0.27	0.27	0.18	0.24	0.30	0.31	0.49	0.44	0.32	0.37	0.65	0.87	0.59	0.55	0.49	0.36	0.48
Yb	0.56	0.71	0.66	0.85	1.77	1.94	1.40	1.62	1.82	1.32	1.38	2.02	2.09	3.09	2.67	2.33	2.38	4.00	5.55	3.83	3.93	3.54	2.55	3.15
Lu	0.08	0.11	0.11	0.15	0.27	0.26	0.24	0.25	0.27	0.17	0.22	0.32	0.36	0.46	0.44	0.33	0.35	0.62	0.92	0.59	0.60	0.56	0.47	0.54

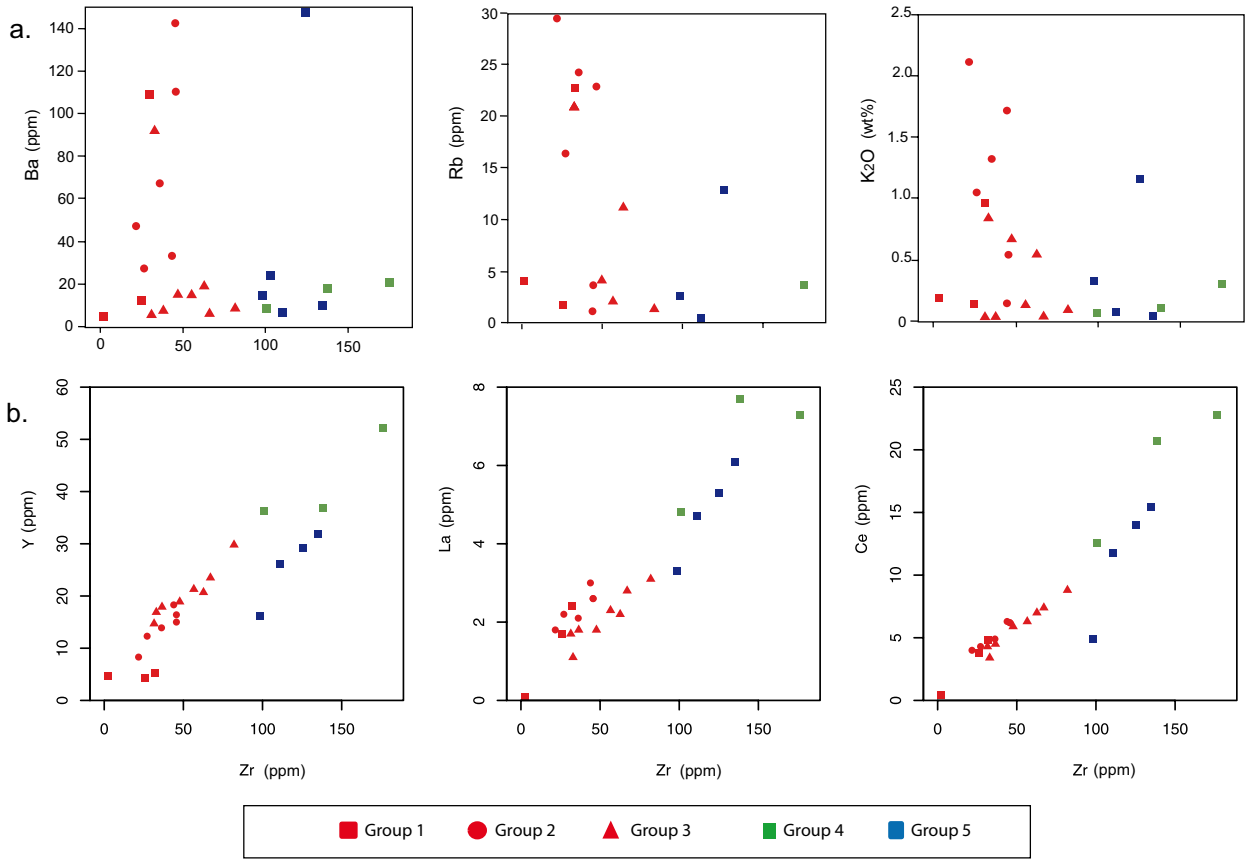

Figure 6. Plots of selected major and trace elements vs. Zr.

Cann, 1973; Floyd and Winchester, 1978) will be used for the geochemical evaluation.

4.3. Geochemical classification

All metamagmatic rocks within the CC show subalkaline affinity (Nb / Y = 0.01–0.16). Based upon the classification diagram (Pearce, 1996), the samples plot into the basalt, basaltic andesite, andesite, and rhyodacite fields (Figure 7). Additionally, these rocks were subdivided into several chemical groups based on their trace element systematics. Within these groups, both primitive and evolved members are present. While Groups 1, 2, and 3 include the primitive samples, Groups 4 and 5 comprise evolved ones.

Group 1 displays geochemical characteristics similar to boninitic rocks with high SiO_2 (54.33–56.35 wt. %) and MgO (10.35–10.68 wt. %) concentrations (Table). The members of this group have higher Zr / Ti (0.01–0.017) and Nb / Y (0.16–0.09) values than the other mafic samples. Groups 2 and 3 mostly plot in the basalt field except for two samples (basaltic andesite), and largely overlap due to their similar Zr / Ti and Nb / Y ratios. Group 4 exhibits andesitic-basaltic andesitic composition (Figure 7), whereas the samples plotting in the rhyodacite field create Group 5 with higher Zr / Ti ratios than the other groups.

In the spider diagrams, Group 1 exhibits highly depleted HFSE contents relative to N-MORB (Nb = 0.1–0.6 ppm, Zr = 2.4–32 ppm; N-MORB Nb = 2.33 ppm, Zr = 74 ppm; Sun and McDonough, 1989). Furthermore, this group shows slightly concave REE patterns (except for DR-11) by enrichments ($[La / Sm]_N$ = 1.48–3.32, where "N" denotes chondrite-normalized) of light rare earth elements (LREEs) and heavy rare earth elements (HREEs) relative to middle rare earth elements (MREEs). Group 2 displays highly depleted Nb concentrations similar to Group 1; however, it appears to be more enriched in terms of the other HFSEs and HREEs (Nb = 0.2–0.7 ppm; Zr = 27.1–47.7 ppm). Group 2 is also characterized by relatively flat to LREE-depleted chondrite-normalized patterns ($[La / Sm]_N$ = 0.68–1.26; Figures 8 and 9). Group 3 displays HFSE (except Nb) and HREE concentrations similar to N-MORB (Nb = 0.6–1.3 ppm; Zr = 56.6–82 ppm) and it exhibits LREE-depleted patterns ($[La / Sm]_N$ = 0.64–0.80) (Figures 8 and 9). Among the evolved groups, Group 4 is characterized by slight depletion in Ti and Eu and displays more enriched patterns in terms of the other HFSEs (Nb = 2–4 ppm; Zr = 100.9–176.2 ppm) and REEs ($[La / Sm]_N$ = 0.80–1.15). However, the second evolved group (Group 5) displays significant anomalies in Ti and Eu and small

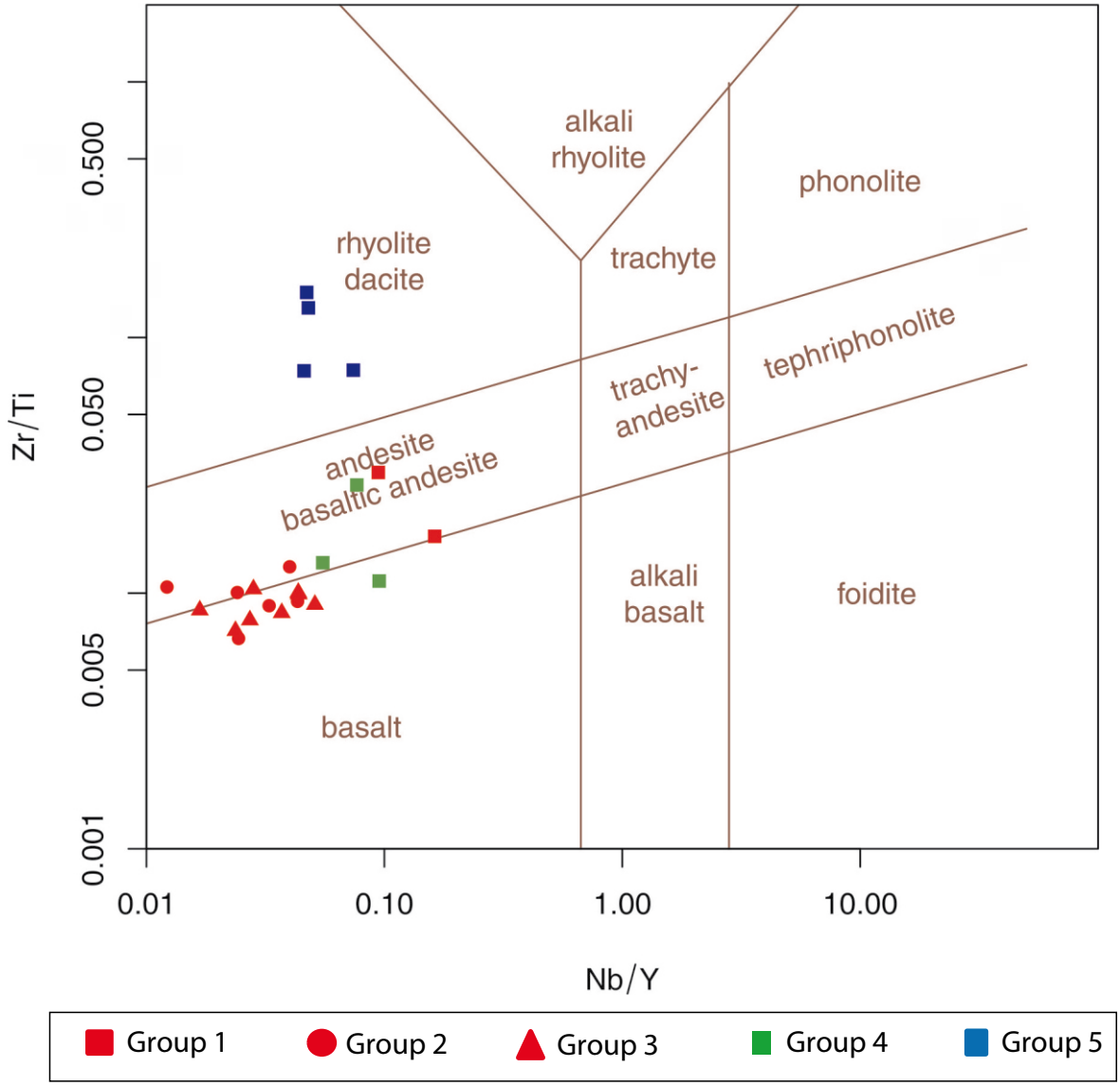

Figure 7. Zr–Ti vs. Nb–Y diagram(after Pearce, 1996) for the metamagmatic rocks of the CC.

enrichments (Figures 8 and 9) in the rest of the HFSEs (Nb = 1.2–3.5 ppm; Zr = 98.3–135) and REEs ($[La / Sm]_N$ = 1.11–2.69).

4.4. Petrogenesis

4.4.1. Fractional crystallization

In order to define the possible effects of fractional crystallization, binary diagrams were used including the rare earth elements Ce, Y, and La and the high field strength element Zr (Figure 6b). When Ce, Y, and La are plotted against Zr, an increasing trend can be traced from the primitive groups towards the evolved ones. It must be noted, however, that Group 4 has overlapping or higher Zr, Ce, Y, and La concentrations than Group 5. The increasing concentrations of the incompatible elements in the evolved members may indicate the role of fractional crystallization during the magmatic evolution. The decreasing concentrations of Cr_2O_3 (Groups 1–3 = 0.06 wt. %; Group 4 = less than 0.002 wt. %; Group 5 = less than 0.002 wt. %) and Ni (Groups 1–3 = 79.90 ppm; Group 4 = 4.26 ppm; Group 5 = 1.40 ppm) from the primitive groups towards the evolved ones also support the idea of fractionation during magmatic processes (Table). The effect of fractional crystallization is best observed in Group

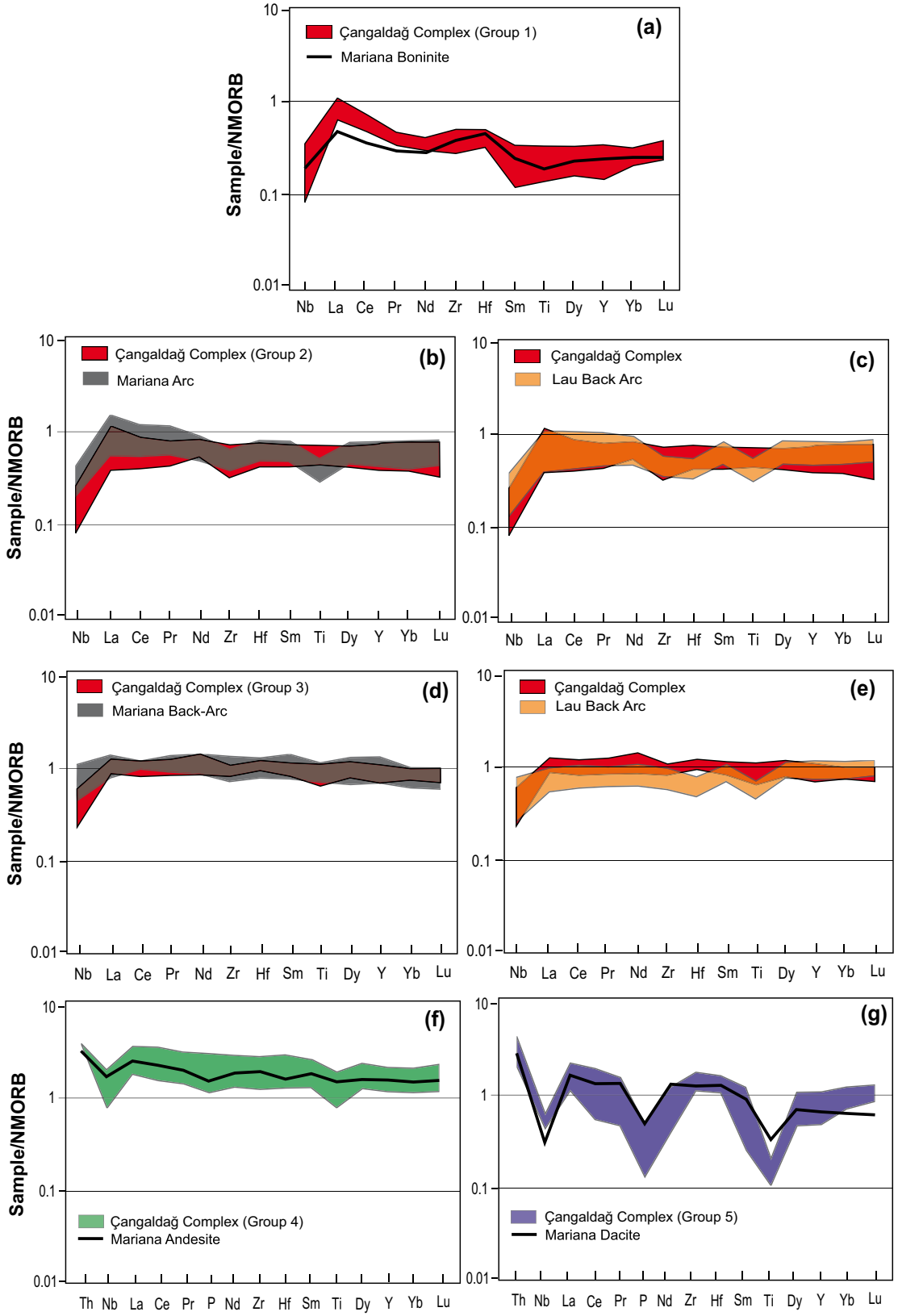

Figure 8. N-MORB normalized spider diagrams (Sun and McDonough, 1989); the data of Mariana and Lau arc-back-arc basin samples are taken from Pearce et al. (1995, 2005).

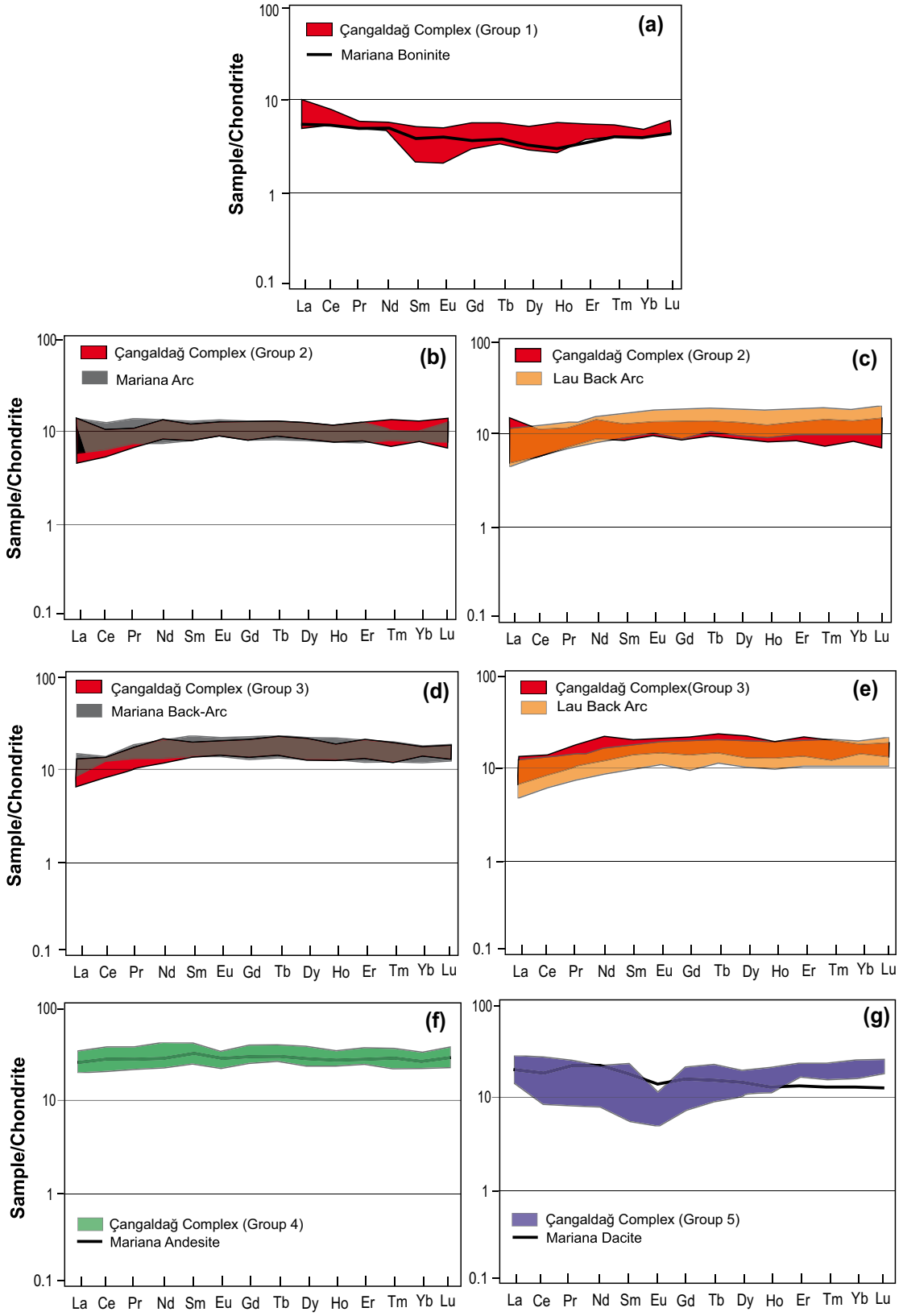

Figure 9. Chondrite-normalized REE diagrams (Sun and McDonough, 1989); the data of Mariana and Lau arc-back-arc basin samples are taken from Pearce et al. (1995, 2005).

5 that displays significant depletions in Ti and Eu, which may suggest fractionation of Ti-oxides and plagioclase. However, it must be noted that Group 5 does not seem to have been evolved from Group 4 due to the lower element enrichment levels (Figures 8 and 9).

4.4.2. Mantle sources

In order to characterize the mantle source(s) of the metamagmatic rocks within the CC, the primitive groups were taken into account to minimize the effects of fractional crystallization. The plots of Zr / Y vs. Nb / Y and La / Yb vs. Zr / Nb ratios can reveal important information related to the possible mantle sources (Figure 10a; Sayit et al., 2016; Figure 10b; Aldanmaz et al., 2000). The lower Zr / Y (0.52–6.04) and Nb / Y (0.02–0.16) values of the Çangaldağ samples indicate derivation from a depleted mantle source (N-MORB Zr / Y = 2.64; Nb / Y = 0.08; Sun and McDonough, 1989). This idea is supported by the lower La / Yb (0.17–3.63) and higher Zr / Nb (37.14–228) ratios, indicating involvement of a depleted mantle source in the petrogenesis of Çangaldağ metamagmatic rocks (N-MORB La / Yb = 0.81; Zr / Nb = 31.75). Such low ratios of Zr / Nb, Zr / Y, and Nb / Y are also found in the basalts of the Mariana arc-back-arc system and Lau Basin in which depleted mantle sources are involved (Figure 10), therefore further reinforcing the idea above.

As mentioned before, Group 1 shows boninite-like characteristics with highly depleted HFSE signatures. The boninitic nature is also confirmed by the similarity of the trace element patterns of Group 1 with the Mariana Arc boninite (Pearce et al., 1992). While such arc-like characteristics of Group 1 suggest the involvement of a subduction component in their mantle source (e.g., Pearce and Peate, 1995), the depletions in HFSEs may indicate different conditions in the mantle source such as stability of minor residual phases (e.g., zircon and titanite; Dixon and Batiza, 1979), remelting of a previously depleted mantle source (Green, 1973; Duncan and Green, 1987; Crawford et al., 1989), or a high degree of partial melting (Pearce and Norry, 1979).

Like Group 1, Group 2 also shows subduction-related characteristics with enrichments in LREEs over HFSEs. This idea is supported by the fact that the Group 2 samples exhibit similar trace element systematics to the basalts from the Mariana Arc and Lau Basin (Pearce et al., 1995, 2005). This indicates that Group 2 has also derived from a subduction-modified mantle source. Group 3 also shares similar geochemical characteristics with the other primitive groups in that it reflects a subduction-related component in their mantle source. The difference, however, is that the overall characteristics of Group 3 samples are rather akin to those generated in back-arcs rather than island arcs. This group also reflects geochemical signatures indicating contribution of slab-derived components (Pearce et al., 1995, 2005).

4.4.3. Partial melting

In order to understand the melting systematics of the primitive metamagmatic rocks from the CC, TiO_2-Yb (Gribble et al., 1998) and Sm vs. Sm / Yb (Sayit et al., 2016) diagrams (Figure 11) were used. In this regard, the samples with MgO concentrations higher than 8 wt. % were used in both diagrams to avoid the effects of fractional crystallization as much as possible.

The modeling plots suggest that the members of Group 1 have been formed at the highest degree of partial melting (higher than 40%) from a spinel or garnet lherzolitic source (Figure 11a). Group 2 follows Group 1 by lower degrees of partial melting with 20%–30%. Group 3, on the other hand, appears to have been formed at the lowest degrees of partial melting among the three with 10%–25%. The extreme values observed in Group 1, however, are rather unrealistic. Instead, remelting from a predepleted mantle source seems more plausible for the petrogenesis of this group (Green, 1973; Duncan and Green, 1987; Crawford et al., 1989). In order to confirm this idea, another diagram was used, which is based on Sm-Yb systematics (Sayit et al., 2016; Figure 11b). This model shows that the Group 1 samples may indeed have been formed by remelting of a predepleted source. In conclusion, while the trace element systematics of Group 2 and 3 metamagmatic rocks can be explained by different degrees of partial melting from a depleted spinel lherzolitic source, the highly depleted characteristics of Group 1 require melting from a predepleted mantle source (Figure 11).

Based on the results above, the increasing degree of enrichments in HFSEs and REEs from Group 1 to Group 3 is more likely to be related to partial melting and previous melt extraction rather than fractional crystallization. In addition, H_2O-rich fluids were reported to have an important role on the degree of melting of the mantle (Davies and Bickle, 1991; Stolper and Newman, 1994; Taylor and Martinez, 2003; Langmuir et al., 2006). Thus, the different degrees of partial melting observed in Group 1, Group 2, and 3 may have been caused by the effect of water derived from the subduction processes (Keller et al., 1992).

4.4.4. Tectonomagmatic discussion

When the Çangaldağ samples with relatively high MgO (i.e. the primitive Groups 1, 2, and 3) are considered, they all exhibit the contribution of a slab-derived component, which is typical in magmas generated in subduction-related settings (Pearce and Peate, 1995). This idea is also supported by the diagrams constructed by Shervais (1982) and Meshede (1986), where the Çangaldağ samples plot in the arc-related regions (Figure 12). Furthermore, all the primitive samples display depleted HFSE and HREE characteristics (N-MORB-like or even lower). When combined with the presence of subduction-related

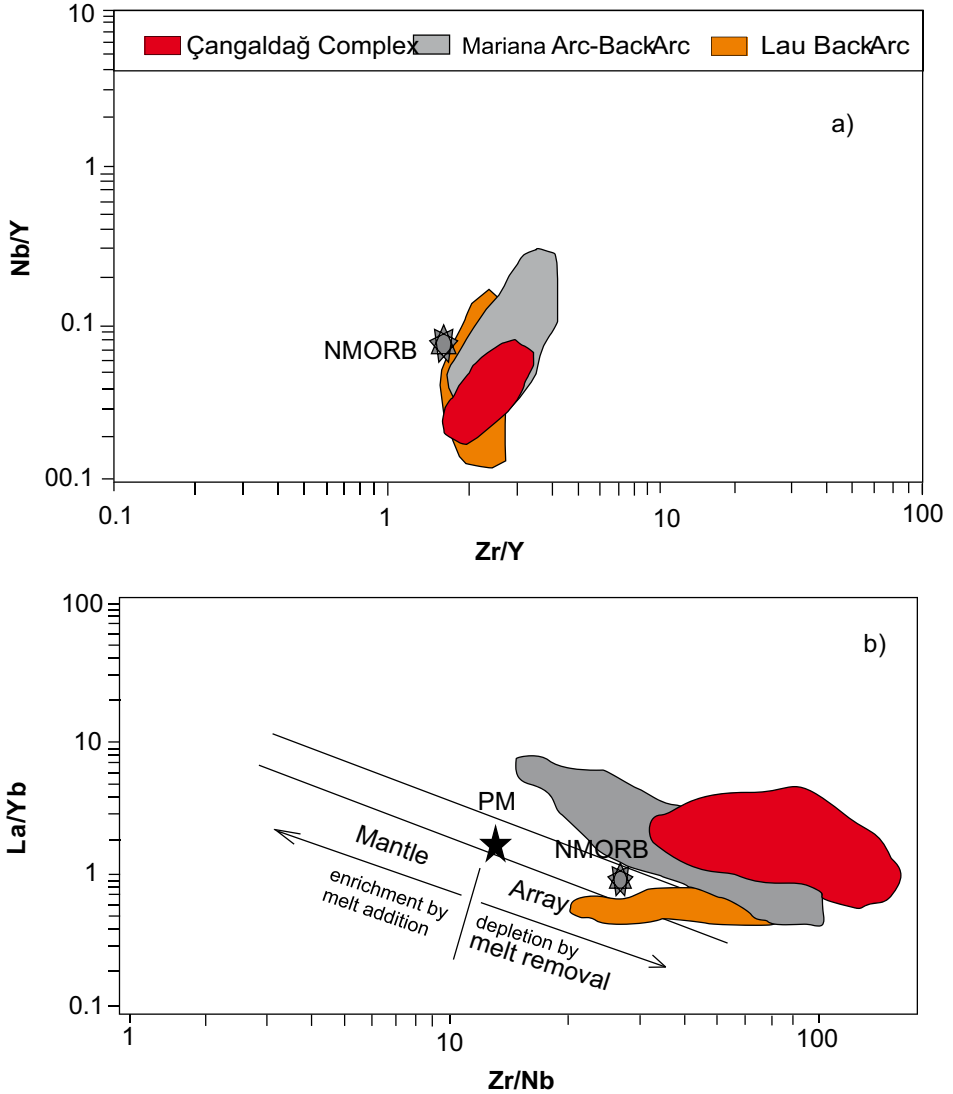

Figure 10. Nb/Y vs. Zr/Y (Sayit et al., 2016) and La/Yb vs Zr/Nb (Aldanmaz et al., 2008) diagrams for the magmatic rocks of the CC; the data of Mariana and Lau arc-back-arc basin samples are taken from Pearce et al. (1995, 2005).

signatures, this may suggest that the Çangaldağ samples may have formed in an intraoceanic subduction system (Pearce et al., 1995; Peate et al., 1997). Among the three groups, however, Groups 1 and 2 possess HFSE and HREE contents apparently lower than N-MORB, suggesting that they may have formed in the arc region of an oceanic arc-basin system. The boninitic Group 1 samples (as also previously described by Ustaömer and Robertson, 1999) are especially indicative of generation at the fore-arc region (Pearce et al., 1992). N-MORB-like features of Group 3, on the other hand, are more consistent with its generation in the back-arc region.

The idea that the Çangaldağ metamagmatic rocks represent the remnants of an intraoceanic arc-basin system as proposed by this study is in general agreement with that of Ustaömer and Robertson (1999), who interpreted the same assemblage to have been generated in an oceanic arc. For instance, the geochemical data previously reported by Ustaömer and Robertson (1999) indicate the presence of basaltic andesite, andesite, dacite, and rhyodacite in the CC. In the discrimination diagrams, these magmatic rocks plot mostly into the island arc tholeiites and MORB fields (Ustaömer and Robertson, 1999). In addition to these rock types, three different primitive groups (basalts) were identified in this study. On the other hand, the geochemical signatures of the back-arc environment, newly reported here, indicate the generation in an arc-back-arc environment rather than a single arc setting. However, the previously thought idea that the CC (similar to the Nilüfer Unit from the Karakaya Complex) represents an oceanic

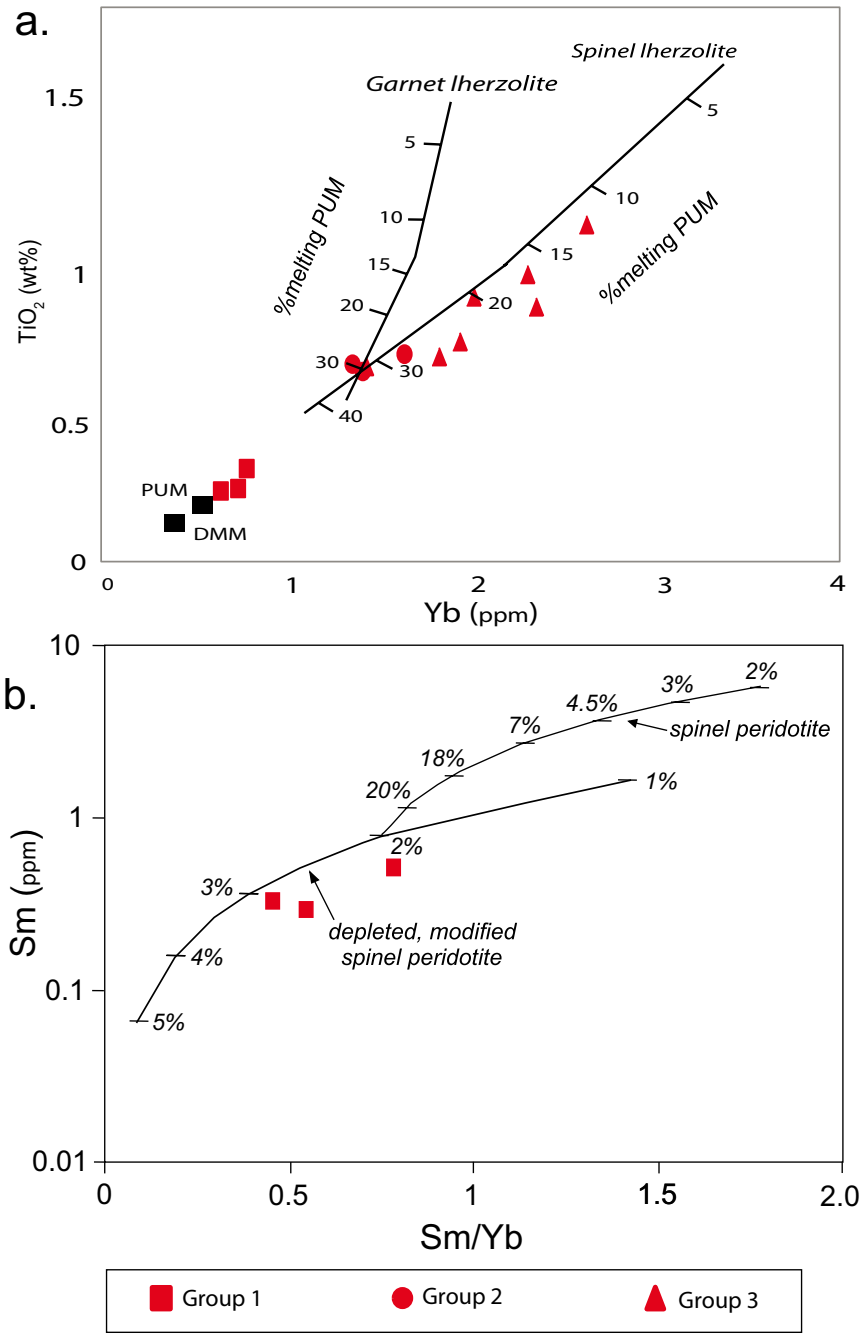

Figure 11. TiO_2 – Yb (Gribble et al., 1998) and Sm vs. Sm/Yb (Sayit et al., 2016) partial melting diagrams for the primitive metamagmatic rocks of the CC (PUM: primitive upper mantle; DMM: depleted MORB mantle).

plateau or oceanic islands (without any geochemical data) as suggested by Okay et al. (2006) is not supported by the present findings. Here it must be noted that this idea was revised as the presence of arc-related magmatism for the origin of the CC by Okay et al. (2013, 2014) by citing the geochemical data that had been already reported in the study of Ustaömer and Robertson (1999). Therefore, the overall geochemical data indicate that the metamagmatic rocks of the CC were likely generated in an intraoceanic arc-back-arc basin environment.

5. Geodynamic discussion

The new geochemical data reported in this paper about the CC play a critical role in understanding the geodynamic

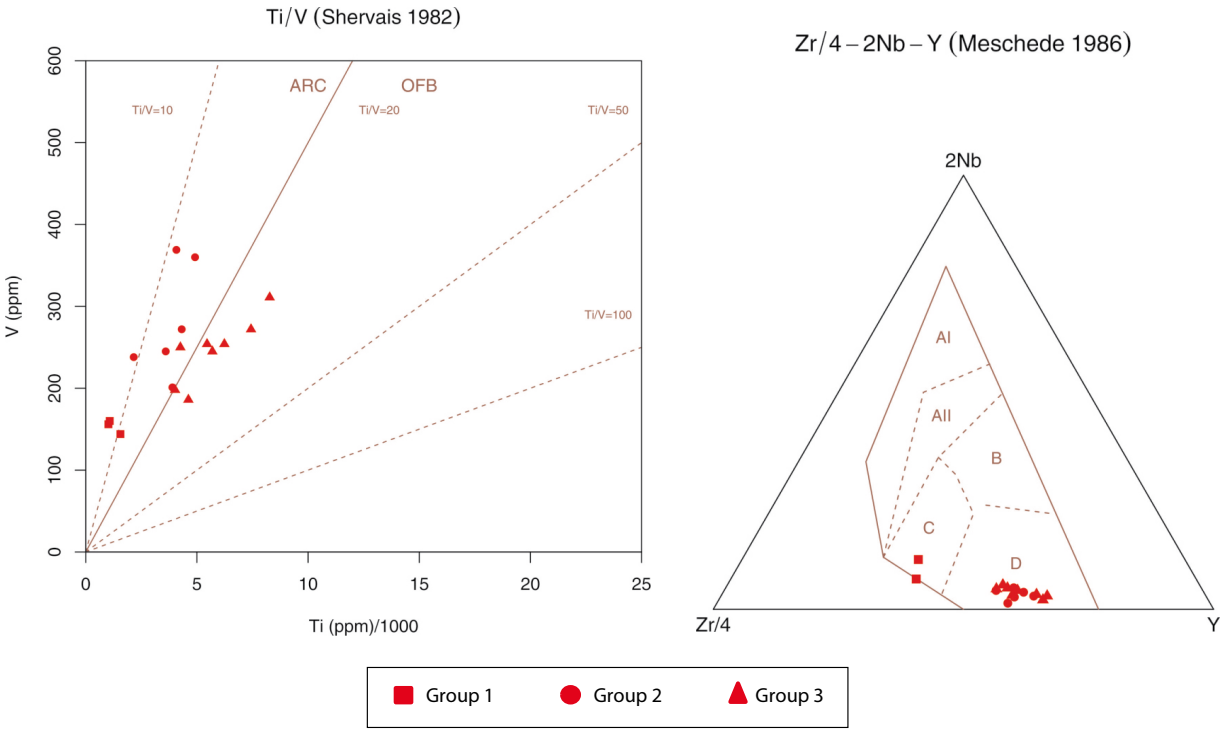

Figure 12. Geotectonic discrimination diagrams: a) after Shervais (1982), b) after Meschede (1986) (AI: within-plate alkali basalt; AII: within-plate tholeiite; B: E-MORB; C and D: volcanic arc basalts; D: N-MORB).

evolution of the Central Pontides. The CC is cropping out between the alpine Sakarya Composite Terrane and İstanbul-Zonguldak Terrane. The presence of two distinct oceanic domains, namely the Paleotethys and the Intra-Pontide branch of the Neotethys between these two terranes during the Middle to Late Mesozoic, is commonly accepted (Kaya, 1977; Şengör and Yılmaz, 1981; Kaya and Kozur, 1987; Yılmaz et al., 1995; Tüysüz, 1999; Elmas and Yiğitbaş, 2001; Robertson and Ustaömer, 2004; Okay et al., 2006, 2008; Göncüoğlu et al., 2008, 2012, 2014; Akbayram et al., 2013; Marroni et al., 2014). However, the paleogeographic and geodynamic settings of these oceans, as well as the lifespans of their oceanic lithosphere, subduction complexes, arcs, etc., are a matter of debate.

In the previous studies, there is consensus that the Küre Complex represents the remnants of the Paleotethyan Küre Basin (sensu Şengör and Yılmaz, 1981). The turbiditic sediments of the complex include Carnian-Norian fossils (Kozur et al., 2000; Okay et al., 2015), indicating that this basin was still open. On the other hand, recent data (Göncüoğlu et al., 2012; Tekin et al., 2012) show that contemporaneously with the closure of the Küre Basin another oceanic branch, the Intra-Pontide Ocean, existed to the south of it. The remains of this ocean cover a vast area in the Central Pontides and are included in the CPSC (Tekin et al., 2012). In general terms, the CPSC is an imbricated stack (e.g., Marroni et al., 2015; Aygül et al., 2016) of accretionary mélanges, dominated by variably deformed and metamorphosed volcanic rocks. Regarding the age, radiolarian data (Göncüoğlu et al., 2010, 2014) from basalt-chert associations indicate that this ocean was partly open until the early Late Cretaceous. Sayit et al. (2016) demonstrated recently that the volcanic rocks within the structurally lower units (Arkot Dağ, Domuz Dağ, Aylı Dağ units) were mainly derived from an intraoceanic subduction system. Our new and detailed evaluation of geochemical data together with additional zircon ages clearly suggests that the CC is a part of this system, as the petrogenetic characteristics of the CC rocks clearly indicate an arc-back-arc basin environment. The IPO basin was obviously larger and older than the intraoceanic subduction event producing the CC volcanism during the Middle Jurassic time (Okay et al., 2014; Çimen et al., 2016b). That it existed prior to the Middle Jurassic is proven by the Middle to Late Triassic oceanic volcanics found in the Arkot Dağ Mélange (Tekin et al., 2012). Moreover, it has not been completely eliminated by the Çangaldağ Mid-Jurassic subduction. This interpretation is supported by the presence of the Late Jurassic MORB-type volcanism in the eastern Bolu area (Göncüoğlu et al., 2008). Additional evidence gives Late Jurassic to early Late Cretaceous radiolarian ages from numerous outcrops within the CC (Göncüoğlu et al., 2012, 2014; Tekin et al., 2012). Considering that the CC tectonically overlies the

Late Jurassic-Cretaceous mélanges with an emplacement direction from N to S, we speculate that they (the Elekdağ, Domuz Dağ, Arkot Dağ, and Aylı Dağ mélanges) were originally located to the S of the Çangaldağ subduction. Another product of Middle Jurassic subduction-related magmatism in Central North Anatolia is represented by the Çangaldağ Pluton. In contrast to the fore-arc-arc-back-arc character of the CC, the Çangaldağ Pluton is a continental arc that intrudes the Küre Complex (Çimen et al., 2016a). All these findings suggest that the IPO has been consumed by multiple intraoceanic subductions as shown in Figure 13.

The geodynamic scenario we propose (Figure 13) is that the volcanic rocks of the CC are products of an island arc system, formed by the northward subduction of a segment of IPO. Moreover, here, the prism 1 may represent the Aylı Dağ ophiolite and Arkot Dağ mélange (including arc-back-arc magmatics; Göncüoğlu et al., 2012); the prism 2 may represent the Domuzdağ, Saka, and Daday units (including again arc-back-arc magmatics; Sayit et al., 2016); and the last subduction zone may have caused the generation of the Çangaldağ Pluton, which displays, as mentioned above, the characteristics of continental arc magmatism (Çimen et al., 2016a; Figure 13). The imbrication of the volcanic assemblages from the fore-arc, the island arc, and the back-arc and their low-grade metamorphism was realized during the Early Cretaceous (Valanginian-Barremian) as evidenced by Ar-Ar white mica ages (Okay et al., 2013). The modern analogues of the CC can found in several places in the world, such as the intraoceanic Mariana arc-basin system, where fore-arc, arc, and back-arc components can be found altogether (Pearce et al., 2005).

The final elimination of the IPO was probably during the Late Cretaceous-Early Tertiary, when its remnants were transported to the south onto the Sakarya Composite Terrane (e.g., Göncüoğlu et al., 2000; Catanzariti et al., 2013; Ellero et al., 2015).

6. Conclusions

The Çangaldağ Complex in the Central Pontides is an imbricated and low-grade metamorphic unit comprising basalts, andesites/basaltic andesites, and rhyodacites with some volcanoclastic rocks. The complex rests with a steep reverse fault on the Tertiary deposits of the Kastamonu-Boyabat Basin and is overthrust by the Çangaldağ Pluton that intrudes into the Küre Complex. Recently, the zircon ICP-MS data from the rhyodacites suggested Middle Jurassic (169 Ma, Okay et al., 2014; 156–176 Ma, Çimen et al., 2016a) ages for the volcanism.

The metamagmatic rocks from the CC include both primitive and evolved members. Trace element systematics of the primitive members suggest that these rocks were derived from a depleted mantle source modified by a subduction-component. While the presence of highly depleted signatures, such as the boninitic ones, indicates an intraoceanic arc origin, the N-MORB-like characteristics are rather consistent with a back-arc origin. Thus, the overall characteristics suggest that Çangaldağ metamagmatic rocks represent remnants of an intraoceanic arc-basin system, including melt generation both in arc and back-arc regions.

These data strongly indicate an intraoceanic arc system with elements from the fore-arc, arc, and back-arc components that were accreted during the closure of a northern segment of the Neotethyan Intra-Pontide Ocean. The evaluation of the petrogenetic features and ages of the variably metamorphic oceanic volcanisms in the Central Pontide Structural Complex imply that the Intra-Pontide Ocean was consumed by stepwise intraoceanic subductions

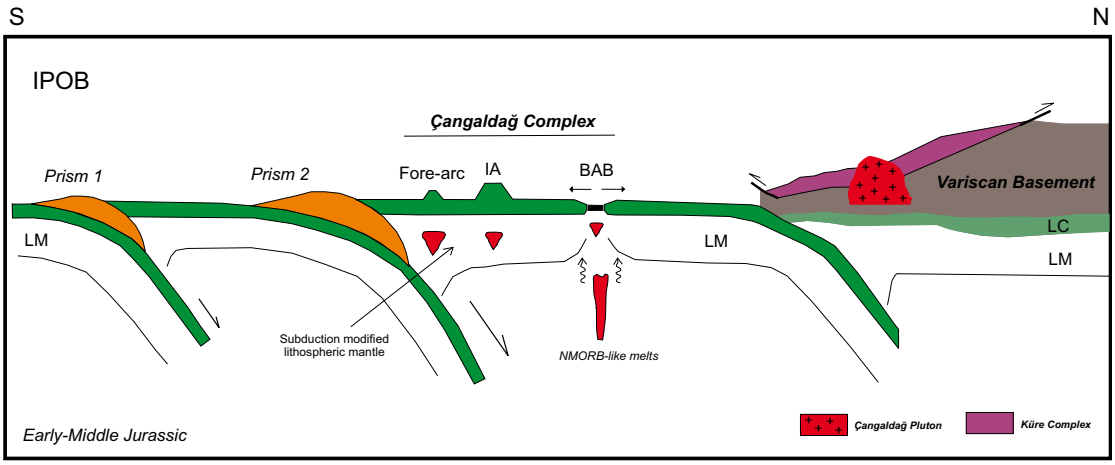

Figure 13. Possible geodynamic model for the Çangaldağ Complex (Prism 1: Aylı Dağ ophiolite and Arkot Dağ Mélange; Prism 2: Domuzdağ, Daday, and Saka Units; LM: lithospheric mantle; IA: island arcs; BAB: back-arc basalts).

giving way to a huge subduction-accretion prism to the N of the Cimmerian Sakarya Composite Terrane.

Acknowledgments
The authors gratefully acknowledge the Higher Educational Council of Turkey for support of this study by the ÖYP project - PhD grant. The authors gratefully acknowledge Dr Gültekin Topuz, Dr Aral Okay, and an anonymous reviewer for their detailed and thoughtful comments, which scientifically improved the manuscript. Also, many thanks to Çağrı Alperen İnan for assistance during field studies.

References

Aldanmaz E, Yalınız MK, Güçtekin A, Göncüoğlu MC (2008). Geochemical characteristics of mafic lavas from the Tethyan ophiolites in western Turkey: implications for heterogeneous source contribution during variable stages of ocean crust generation. Geol Mag 145: 37-54.

Aydın M, Demir O, Özçelik Y, Terzioğlu N, Satır M (1995). A geological revision of İnebolu, Devrekani, Ağlı and Küre areas: New observations in Paleo-Tethys - Neo-Tethys sedimentary successions. In: Erler A, Ercan T, Bingöl E, Örçen S, editors. Geology of the Black Sea Region. Ankara, Turkey: MTA/JMO, pp. 33-38.

Aydın M, Şahintürk Ö, Serdar HS, Özçelik Y, Akarsu İ, Üngör A, Çokuğraş R, Kasar S (1986). Ballıdağ-Çangaldağı (Kastamonu) arasındaki bölgenin jeolojisi. TJK Bülteni 29: 1-16 (in Turkish).

Aygül M, Okay AI, Oberhänsli R, Sudo M (2016). Pre-collisional accretionary growth of the southern Laurasian active margin, Central Pontides, Turkey. Tectonophysics 671: 218-234.

Boztuğ D, Debon F, Le Fort P, Yılmaz O (1995). High compositional diversity of the Middle Jurassic Kastamonu Plutonic Belt, northern Anatolia, Turkey. Turk J Earth Sci 4: 67-86.

Boztuğ D, Yılmaz O (1995). Daday-Devrekani masifi metamorfizması ve jeolojik evrimi, Kastamonu bölgesi, Batı Pontidler, Türkiye. TJK Bülteni 38: 33-52 (in Turkish).

Catanzariti R, Ellero A, Göncüoğlu MC, Marroni M, Ottria G, Pandolfi L (2013). The Taraklı Flysch in the Boyali area (Sakarya Terrane, northern Turkey): implications for the tectonic history of the IntraPontide suture zone. C R Geosci 345: 454-461.

Çimen O, Göncüoğlu MC, Sayıt K, Simonetti A (2016a). Whole rock geochemistry, U-Pb geochronology and Lu-Hf isotope systematics of the Çangaldağ Pluton (Central Pontides, Turkey). In: 69th Geological Congress of Turkey, Abstracts and Program, pp. 148-149.

Çimen O, Göncüoğlu MC, Simonetti A, Sayıt K (2016b). Zircon U-Pb geochronology, Hf isotopes and whole rock geochemistry of the meta-magmatic rocks from the Çangaldağ Complex (Central Pontides, Turkey). In: 69th Geological Congress of Turkey, Abstracts and Program, pp. 269-270.

Crawford AJ, Falloon TJ, Green DH (1989). Classification, petrogenesis and tectonic setting of boninites. In: Crawford AJ, editor. Boninites. London, UK: Unwin Hyman, pp. 1-49.

Davies JH, Bickle MJ (1991). A physical model for the volume and composition of melt produced by hydrous fluxing above subduction zones. Philos T R Soc 335: 355-364.

Dixon TH, Batiza R (1979). Petrology and chemistry of recent lavas in the Northern Marianas: implications for the origin of island arc basalts. Contrib Mineral Petrol 70: 167-181.

Duncan RA, Green DH (1987). The genesis of refractory melts in the formation of oceanic crust. Contrib Mineral Petrol 96: 326-342.

Ellero A, Ottria G, Sayit K, Catanzariti R, Frassi C, Göncüoğlu MC, Marroni M, Pandolfi L (2015). Geological and geochemical evidence for a Late Cretaceous continental arc in the central Pontides, northern Turkey. Ofioliti 40: 73-90.

Floyd PA, Winchester JA (1978). Identification and discrimination of altered and metamorphosed volcanic rocks using immobile elements. Chem Geol 21: 291-306.

Floyd PA, Winchester JA, Seston R, Kryza R, Crowley QG (2000). Review of geochemical variation in Lower Palaezoic metabasites from the NE Bohemian Massif; intracratonic rifting and plume ridge interaction. In: Franke W, Haak V, Oncken O, Tanner D, editors. Orogenic Processes: Quantifications and Modeling in the Variscan Belt. London, UK: Geological Society of London Special Publication 179, pp. 155-174.

Göncüoğlu MC (2010). Introduction to the Geology of Turkey: Geodynamic Evolution of the Pre-Alpine and Alpine Terranes. Ankara, Turkey: MTA.

Göncüoğlu MC, Gürsu S, Tekin UK, Köksal S (2008). New data on the evolution of the Neotethyan oceanic branches in Turkey: Late Jurassic ridge spreading in the Intra-Pontide branch. Ofioliti 33: 53-164.

Göncüoğlu MC, Kozlu H, Dirik K (1997). Pre-Alpine and Alpine terranes in Turkey: explanatory notes to the terrane map of Turkey. Ann Geol Pays Helleniques 37: 515-536.

Göncüoğlu MC, Marroni M, Pandolfi L, Ellero A, Ottria G, Catanzariti R, Tekin UK, Sayit K (2014). The Arkot Dağ Melange in Araç area, central Turkey: evidence of its origin within the geodynamic evolution of the Intra-Pontide suture zone. J Asian Earth Sci 85: 117-139.

Göncüoğlu MC, Marroni M, Sayit K, Tekin UK, Ottria G, Pandolfi L, Ellero A (2012). The Aylı Dağ ophiolite sequence (Central-Northerm Turkey): a fragment of Middle Jurassic Oceanic Lithosphere within the Intra-Pontide suture zone. Ofioliti 37: 77-92.

Göncüoğlu MC, Sayit K, Tekin UK (2010). Oceanization of the northern Neotethys: geochemical evidence from ophiolitic melange basalts within the Izmir–Ankara suture belt, NW Turkey. Lithos 116: 175-187.

Göncüoğlu MC, Turhan N, Sentürk K, Özcan A, Uysal S (2000). A geotraverse across NW Turkey: tectonic units of the Central Sakarya region and their tectonic evolution. In: Bozkurt E, Winchester JA, Piper JD, editors. Tectonics and Magmatism in Turkey and the Surrounding Area. London, UK: Geological Society of London Special Publication 173, pp. 139-162.

Green DH (1973). Experimental melting studies on a model upper mantle composition at high pressure under water-saturated and water-unsaturated conditions. Earth Planet Sci Letter 19: 37-53.

Gribble RF, Stern RJ, Newman S, Bloomer SH, O'Hearn T (1998). Chemical and isotopic composition of lavas from the northern Mariana Trough; implications for magma genesis in back-arc basins. J Petrol 39: 125-154.

Gücer MA, Arslan M (2015). Petrochemistry, petrology, geochronology and P-T estimation of the Devrekani (Kastamonu, N Turkey) Massif. In: 25th Anniversary Goldschmidt Conference, Abstracts, p. 1113.

Gücer MA, Arslan M, Sherlock S, Heaman LM (2016). Permo-Carboniferous granitoids with Jurassic high temperature metamorphism in Central Pontides, Northern Turkey. Miner Petrol: 1-22.

Kaya MY, Altıner D (2014). *Terebella lapilloides* Münster, 1833 from the Upper Jurassic-Lower Cretaceous İnalti carbonates, northern Turkey: its taxonomic position and paleoenvironmental paleoecological significance. Turk J Earth Sci 23: 166-183.

Keller RA, Fisk MR, White WM, Birkenmajer K (1992). Isotope and trace element constraints on mixing and melting models of marginal basin volcanism, Barnsfield Strait, Antarctica. Earth Planet Sci Letter 111: 287-303.

Konya S, Pehlivanoğlu H, Teşrekli M (1988). Kastamonu, Taşköprü, Devrekani Yöresi Jeokimya Raporu. Ankara, Turkey MTA (in Turkish).

Kozur H, Aydın M, Demir O, Yakar H, Göncüoğlu MC, Kuru F (2000). New stratigraphic results from the Paleozoic and Early Mesozoic of the Middle Pontides (Northern Turkey). Geol Croat 53: 209-268.

Langmuir CH, Bézos A, Escrig S, Parman SW (2006). Chemical systematics and hydrous melting of the mantle in back-arc basins. In: Christie DM, Fisher CR, Lee SM, Givens S, editors. Back-Arc Spreading Systems: Geological, Biological, Chemical and Physical Interactions, Volume 166. Hoboken, NJ, USA: Wiley, pp. 87-146.

Marroni M, Frassi C, Göncüoğlu MC, Di Vincenzo G, Pandolfi L, Rebay G, Ellero A, Ottaria G (2014). Late Jurassic amphibolite-facies metamorphism in the Intra-Pontide Suture Zone (Turkey): an eastward extension of the Vardar Ocean from the Balkans into Anatolia? J Geol Soc 171: 605-608.

Meschede M (1986). A method of discriminating between different types of midocean ridge basalts and continental tholeiites with the Nb-Zr-Y diagram. Chem Geol 56: 207-218.

Okay AI, Altıner D, Kılıç A (2015). Triassic limestone, turbidites and serpentinite–the Cimmeride orogeny in the Central Pontides. Geol Mag 152: 460-479.

Okay AI, Gürsel S, Sherlock S, Altıner D, Tüysüz O, Kylander-Clark ARC, Aygül M (2013). Early Cretaceous sedimentation and orogeny on the active margin of Eurasia: Southern Central Pontides, Turkey. Tectonics 32: 1247-1271.

Okay AI, Gürsel S, Tüysüz O, Sherlock S, Keskin M, Kylander-Clark ARC (2014). Low-pressure - high-temperature metamorphism during extension in a Jurassic magmatic arc, Central Pontides, Turkey. J Metamorph Geol 32: 49-69.

Okay AI, Nikishin MA (2015). Tectonic evolution of the southern margin of Laurasia in the Black Sea region. Int Geol Rev 57: 1051-1076.

Okay AI, Tüysüz O (1999). Tethyan sutures of northern Turkey, in the Mediterranean Basins: Tertiary extension within the Alpine Orogen. Geol Soc London Spec Publ 156: 475-515.

Okay AI, Tüysüz O, Satır M, Özkan-Altıner S, Altıner D, Sherlock S, Eren RH (2006). Cretaceous and Triassic subduction-accretion, high-pressure-low-temperature metamorphism, and continental growth in the Central Pontides, Turkey. GSA Bull 118: 1247-1269.

Pearce JA (1975). Basalt geochemistry used to investigate past tectonic environments on Cyprus. Tectonophysics 25: 41-67.

Pearce JA (1996). A users guide to basalt discrimination diagrams. In: Wyman DA, editor. Trace Element Geochemistry of Volcanic Rocks: Applications for Massive Sulphide Exploration. Short Course Notes 12. St. John's, Canada: Geological Association of Canada, pp. 79-113.

Pearce JA, Cann JR (1973). Tectonic setting of basic volcanic rocks determined using trace element analyses. Earth Planet Sci Letter 19: 290-300.

Pearce JA, Ernewein M, Bloomer SH, Parson LM, Murton BJ, Johnson LE (1995). Geochemistry of Lau Basin volcanic rocks: influence of ridge segmentation and arc proximity. In: Smellie JL, editor. Volcanism Associated with Extension at Consuming Plate Margins. London, UK: Geological Society of London Special Publication 81, pp. 53-75.

Pearce JA, Norry M (1979). Petrogenetic implications of Ti, Zr, Y and Nb variations in volcanic rocks. Contrib Mineral Petrol 69: 33-47.

Pearce JA, Peate DW (1995). Tectonic implications of the composition of volcanic arc magmas. Annu Rev Earth Pl Sc 23: 251-286.

Pearce JA, Stern RJ, Bloomer SH, Fryer P (2005). Geochemical mapping of the Mariana arc-basin system: Implications for the nature and distribution of subduction components. Geochem Geophys Geosyst 6: Q07006.

Pearce JA, van der Laan SR, Arculus RJ, Murton BJ, Ishii T, Peate DW, Parkinson IJ (1992). Boninite and harzburgite from Leg 125 (Bonin-Mariana forearc): a case study of magma genesis during the initial stages of subduction. Proc Ocean Drill Prog Sci Res 125: 623-659.

Peate DW, Pearce JA, Hawkesworth CJ, Collie H, Edwards CHM, Hirose K (1997). Geochemical variations in Vanuatu arc lavas: the role of subducted material and a variable mantle wedge composition. J Petrol 38: 1331-1358.

Perfit MR, Fornari DJ (1983). Geochemical studies of abyssal lavas recovered by DSRV ALVIN from the eastern Galapagos Rift - Inca Transform - Ecuador Rift: II. Phase chemistry and crystallization history. J Geophys Res 88: 530-550.

Robertson A, Parlak O, Ustaömer T, Taslı K, İnan N, Dumitrica P, Karaoğlan F (2014). Subduction, ophiolite genesis and collision history of Tethys adjacent to the Eurasian continental margin: new evidence from the Eastern Pontides, Turkey. Geodin Acta 26: 230-293.

Sayit K, Marroni M, Göncüoğlu MC, Pandolfi L, Ellero A, Ottria G, Frassi C (2016). Geological setting and geochemical signatures of the mafic rocks from the Intra-Pontide Suture Zone: implications for the geodynamic reconstruction of the Mesozoic Neotethys. Int J Earth Sci 105: 39-64.

Şen Ş (2013). New evidences for the formation of and for petroleum exploration in the fold-thrust zones of the central Black Sea Basin of Turkey. Am Assoc Petrol Geol Bull 97: 465-485.

Şengör AMC, Yılmaz Y (1981). Tethyan evolution of Turkey: a plate tectonic approach. Tectonophysics 75: 181-241.

Şengün M, Akçaöre F, Keskin H, Akat U, Altun İE, Deveciler E, Sevin M, Armağan F, Erdoğan K, Acar Ş et al. (1988). Daday-Kastamonu-İnebolu Yöresinin Jeolojisi. Ankara, Turkey: MTA Raporu No: 8994 (in Turkish).

Shervais JW (1982). Ti–V plots and the petrogenesis of modern ophiolitic lavas. Earth Planet Sci Lett 59: 101-118.

Stolper E, Newman S (1994). The role of water in the petrogenesis of Mariana trough magmas. Earth Planet Sci Lett 121: 293-325.

Sun SS, McDonough WF (1989). Chemical and isotopic systematics of oceanic basalts: implications for mantle composition and processes. Geol Soc London Spec Publ 42: 313-345.

Taylor B, Martinez F (2003). Back-arc basin basalt systematics. Earth Planet Sci Lett 210: 481-497.

Tekin UK, Göncüoğlu MC, Pandolfi L, Marroni M (2012). Middle Late Triassic radiolarian cherts from the Arkotdağ melange in northern Turkey: implications for the life span of the northern Neotethyan branch. Geodin Acta 25: 305-319.

Tüysüz O (1985). Kargı Masifi ve dolayındaki tektonik birliklerin ayırdı ve araştırılması (petrolojik inceleme). PhD, İstanbul University, İstanbul, Turkey (in Turkish).

Tüysüz O (1990). Tectonic evolution of a part of the Tethyside orogenic collage: The Kargı Massif, northern Turkey. Tectonics 9: 141-160.

Uğuz MF, Sevin M (2007). Türkiye Jeoloji Haritaları, Kastamonu-E32 Paftası. Ankara, Turkey: Jeoloji Etütleri Dairesi (in Turkish).

Ustaömer T, Robertson AHF (1993). A late Palaeozoic-Early Mesozoic marginal basin along the active southern continental margin of Eurasia: evidence from the Central Pontides (Turkey) and adjacent regions. Geol J 28: 219-238.

Ustaömer T, Robertson AHF (1994). Late Palaezoic marginal basin and subduction-accretion: the Palaeotethyan Küre Complex, Central Pontides, northern Turkey. J Geol Soc London 151: 291-305.

Ustaömer T, Robertson AHF (1999). Geochemical evidence used to test alternative plate tectonic models for pre-Upper Jurassic (Palaeotethyan) units in the Central Pontides, N Turkey. Geol J 34: 25-53.

Wood DA, Gibson IL, Thompson RN (1976). Elemental mobility during zeolite facies metamorphism of the Tertiary basalts of eastern Iceland. Contrib Mineral Petrol 55: 241-254.

Yılmaz O (1980). Daday-Devrakani masifi kuzeydoğu kesimi litostratigrafi birimleri ve tektoniği. Yerbilimleri 5: 101-135 (in Turkish).

Yılmaz O (1983). Çangal metaofiyolitinin mineralojik-petrografik incelenmesi ve metamorfizma koşulları. Yerbilimleri 10: 45-58 (in Turkish).

Yılmaz O (1988). L'ensemble ophiolitique de Çangal (Turquie du Nord): Mise en évidence d'un métamorphisme océanique et d'un rétrométamorphisme cataclastique tardif. Geologie Alpine 64: 113-132 (in French with abstract in English).

Yılmaz O, Bonhomme MG (1991). K-Ar isotopic age evidence for a Lower to Middle Jurassic low-pressure and a Lower Cretaceous high-pressure metamorphic events in north-central Turkey. Terra Abstracts 3: 501.

Yılmaz Y, Tüysüz O (1984). Kastamonu-Boyabat-Vezirköprü-Tosya Arasındaki Bölgenin Jeolojisi (Ilgaz-Kargı Masiflerinin Etüdü). Ankara, Turkey: MTA Raporu No. 7838 (in Turkish).